

SLANTED-AXIS ANTENNA DESIGN I

Jingquan Cheng
June, 14 1993

ABSTRACT

This is the first part of the slanted-axis MMA antenna design report. General design of the antenna structure is provided. Some preliminary static and dynamic analysis results are included. However, this part excludes the thermal and wind analysis which form other important parts of the antenna design study.

The proposed design has a homologically deformed rigid backup structure, which is supported by a 45 degree tilted bearing ring. The receiver cabin is located at the other side of the slanted bearing ring, above the azimuth bearing. This design has a higher rigidity, lower overall weight and more stable receiver position than the standard Cassegrain. However, it involves complex coordinate transformation, undesirable slanted bearing force condition and difficulties in accommodating an on axis slanted axis encoder. This report gives the preliminary calculation of the weight, stress, frequency range and error estimation. In the same report, the comparison between this design and classical Cassegrain or bent-Nasmyth design is also provided.

CONTENTS

1. ANTENNA REQUIREMENTS REVIEW

- 1.1 Antenna specifications
- 1.2 Environmental conditions
- 1.3 Other considerations of the MMA antenna

2. ANTENNA STRUCTURAL DESIGN STRATEGY

- 2.1 General structural considerations
- 2.2 Considerations of backup structure design
- 2.3 Advantages of slanted-axis structure
- 2.4 Disadvantages of slanted-axis design

3. GENERAL DESIGN OF A SLANTED-AXIS ANTENNA

- 3.1 Antenna arrangement
- 3.2 Preliminary weight distribution
- 3.3 Panel design
- 3.4 Backup structure design
- 3.5 Secondary mirror support design
- 3.6 Slanted-axis structure design
- 3.7 Receiver cabin design
- 3.8 Antenna base design
- 3.9 Drive and encoder considerations
 - 3.9.1 secondary mirror drive
 - 3.9.2 Turntable drive
 - 3.9.3 Encoder system

4. DYNAMIC ANALYSIS OF THE STRUCTURE

- 4.1 NASTRAN model
- 4.2 Loadings for analysis

- 4.3 NASTRAN dynamic analysis results of the design**
- 4.4 Comparison with Cassegrain and bent-Nasymth design**
- 4.5 Dynamic requirements for fast switching**

5. STATIC GRAVITATION ANALYSIS OF THE STRUCTURE

- 5.1 Backup structure arrangement**
- 5.2 Formulas of parabolic surface fitting**
- 5.3 Parabolic surface error under gravitation force**
- 5.4 Static stress calculation under surviving condition**

APPENDIX Stiffness of Serrurier-type truss structure

1.2 Environmental conditions

In the previous paragraph, it is stated that MMA antenna should be able to work day and night all year around. However, for some severe wind, rain and snow conditions the observation made by using the future MMA will result in very few meaningful results. Furthermore the cost consideration of the project will eventually set a limit for the allowable working condition. Therefore, it is necessary to compromise between design engineers and MMA future users. The problems which need to be answered are:

1) what is the worst condition the antenna should work without degrading its operation precision or what is the percentage of time on a particular site the antenna should work without degrading its operation precision?

2) what is the condition in which the antennas should work with a degraded precision or what percentage of time on a particular site should the antennas work with a degraded precision?

3) what are the conditions the antenna can survive?

Different sites have different environmental conditions. Among three possible MMA sites, wind data for Magdalena mountain(3,200 m (10,500 feet) elevation) and Springerville(2,800 m (9,200 feet) elevation) are from Hogg^[3] and those of Mauna Kea(3,800 m(12,500 feet) elevation) are from Cheimets^[4]. Maximum wind speed recorded at these three sites are 100, 64 and 110 mph respectively. These speed in MKS unit are 45, 29 and 50 m/s respectively. Among three sites, wind speed is below 15 m/s 90% of the time. But for some percentage of time, the wind speed can reach 25 m/s or more. Therefore it is suggested that antenna working conditions should be as follows. These specifications are similar to those for SMA antennas^[6].

| | |
|---------------------|-------------------------|
| Wind speed range 1 | 1- 14 m / s (1- 30 mph) |
| Wind speed range 2 | 14 - 20 m / s |
| Wind speed range 3 | 20 - 25 m / s |
| Temperature range 1 | -15 to +25 C |
| Temperature range 2 | -20 to +30 C |
| Solar loading | 1260 W / m ² |

Within the working conditions, Range 1 should be the one where the antenna should operate without degrading its operation precision and other ranges will be those where the antenna will operate with degraded precision. The suggested designed survival conditions are:

1. ANTENNA REQUIREMENTS REVIEW

1.1 Antenna specification^{[1][2]}

The Millimeter Array(MMA) is designed as a complete powerful image instrument composed of forty 8 meter diameter precision antennas. With different array baselines, the MMA can achieve a highest angular resolution, less than 0.007", and also wide angle images of large regions of the sky with a lower angular resolution. In doing so, from time to time a phase calibration has to be performed for each antenna within the array. This particular requirement demands the antenna should be rigid enough, the moment of its moving part should be low enough or the driving power should be large enough to accommodate this rapid back and forth switching from the object to a nearby calibrator for many hours a day all year around. Besides, the MMA is also required to be able to work all times of the day and night, which includes those time periods facing wind and severe thermal environment conditions. Furthermore, the MMA is also required to be able to observe the sun directly. For penetrating most of the atmosphere which absorbs radiation over the millimeter wave range, the array will be sited above 2750 meters(~9,000 feet) in elevation. In summary, the basic antenna specifications for the MMA array are as follows:

| | |
|--|----------------------|
| Number of antennas | 40 |
| Nominal reflector size | 8 m |
| Frequency range | 30-370 GHz |
| Total surface rms error | 25 μ m |
| Pointing error | 1 " |
| Fast switching range | 1.5 deg |
| Fast switching period | 6 sec |
| Fast switching acceleration | (to be determined) |
| Sky coverage | > 5 deg in elevation |
| Solar observation | yes |
| Transportable | yes |
| Minimum separation between antennas | ~ 10 m |
| Operation time | day and night |
| site altitude | >2750 m |
| Minimum cost | yes |

| | |
|--------------|-----------------------------|
| Wind speed | 60 m/s (134 mph) |
| Rain | 10 cm per hour for one hour |
| Snow | 0.5 m |
| snow loading | 160 kg/m ³ |
| Ice | 10 cm on flat surface |
| | 7.5 cm on tubular structure |
| ice loading | 913 kg/m ³ |

1.3 Other considerations of the MMA antenna

Other considerations of the MMA antenna design include the antenna optics arrangement, manufacturing and operational requirements. The basic optical parameters of the system are primary focal ratio, secondary focal ratio and the back focus distance. These three parameters are selected by considering the antenna efficiency and structural feasibility. In summary, additional considerations are:

| | |
|---------------------------|--|
| Primary focal ratio | ~ 0.4 |
| Secondary focal ratio | ~ 12 (for matching the receiver pattern) |
| Secondary mirror diameter | ~ 0.6 m |
| Back focus distance | < 5 m |
| Receiver condition | stable and accessible |
| Receiver size | >1 x 1 x 1 m |
| Maintenance | minimum |
| Mass production | yes |

2. ANTENNA STRUCTURAL DESIGN STRATEGY

2.1 General structural considerations

By considering the antenna system focal ratio and the diameter of its secondary mirror, the preferred optical arrangements are Cassegrain or Nasmyth optics. These optical arrangements all have a short back focus distance and a small secondary mirror diameter. A slanted-axis optics is similar to a Nasmyth one: its back focus distance is also short. Therefore we could choose the slanted-axis concept as the candidate for the MMA antenna design. Cassegrain or Nasmyth optics have been adapted by BIMA^[5] and SMA^[6] projects where the antennas designed have similar optical requirements to the MMA antennas (note: SMA antennas use a bent-Nasmyth arrangement since a classical Nasmyth arrangement

results in a bigger sweeping volume). In this design study, these two types of arrangements(Cassegrain and bent-Nasymth) are also discussed.

Besides the optical system arrangement, there are three other important considerations for the MMA antenna structure design. The first is the antenna surface accuracy, which is mostly connected to the backup structure design. The backup structure should have a homological deflection pattern when it is under the gravitational field. However, minimizing the interaction between other structures and the backup structure is also important in order to maintain homology of the surface shape. The second consideration in the design is to maintain a higher pointing accuracy. Mechanical deformation is one source in pointing errors. But most of mechanical deformations are repeatable. The pointing errors which are not repeatable are mainly from wind and temperature gradients. To reduce wind induced pointing error, the structure should be rigid, and to reduce thermal induced pointing error, some extent of passive(preferred) or active temperature control may be required. The third consideration of the design is to accommodate the rapid back and forth calibration switching. The structure settling time is inversely proportional to structural natural frequency. To reduce the settling time, again the antenna structure should be more rigid and the moment of rotating parts should be small. In this way, quicker response to the control loop would be possible. Specifically, general design considerations of the MMA antenna are:

- * To design a rigid structure with minimum weight;
- * To reduce the moment of inertia of the moving parts of the antenna;
- * To use durable and reliable surface panels;
- * To use Carbon Fiber Reinforce Plastics (CFRP) as the main material for the backup structure to match the severe thermal design requirement;
- * Try to design an open backup structure unless the thermal distortion is too big during working conditions; The advantages of an open backup structure are light weight, smaller thermal time constant, possibly smaller wind induced drag force, easier manufacture and maintenance.
- * Separate backup structure with its supporting structure so that the deformation of the supporting structure will only affect the pointing error but not the surface shape;
- * Insulate the base structure to reduce thermal pointing error;

2.2 Considerations of backup structure design

The backup structure is a most important component in the antenna design. It supports the surface panels which reflect the radiation from the source to the receiver. The deviation of reflecting panels away from a perfect parabola affects the overall efficiency of the antenna^[7]. Surface errors caused by backup structure are from gravitational field, wind loads and thermal gradients. To reduce wind induced error, the structure should be stiff. To reduce thermal induced error, one has to reduce the thermal gradients within the structure

and to use a low thermal expansion material. An open structure with nearly uniform member size will be helpful in the former aspect. Gravitational surface errors are predictable and are determined by geometry, topology and member section area of the backup structure. To reduce gravitational surface error, the best way is still trial and error. By considering the thermal performance, a central hub supported backup structure is not preferred. Also the cost of the antenna will be reduced if a uniform cross-section area is used. Specifically, the considerations of the backup structure design are:

- * Minimizing the number of nodes in the structure; In CFRP design, nodes are a significant portion of the backup structure weight but they do not help to increase its stiffness.
- * Applying space truss to the structure which has maximum stiffness to weight ratio compared with a plane truss structure;
- * Try to use a uniform cross section for most of the structure members to reduce the cost of the antenna;
- * To design a strong and stable main frame for the supporting points and separate the deflection effect between backup structure and its supporting structure;
- * Separating the secondary mirror support structure from the backup structure;
- * Avoiding central hub and reducing thermal time constant.

2.3 Advantages of slanted-axis structure

In this report, the slanted-axis concept is selected. The slanted-axis concept was firstly suggested by Lamb and Payne. The concept has been discussed by Cheng^[8]. The main advantages of adopting a slanted-axis design is its higher stiffness compared to both Cassegrain or bent-Nasmyth(adapted by SMA antenna) design. Therefore the structure designed can have a higher natural frequency. Other advantages of this new concept are:

- * The counterweight of the backup structure used for most antenna designs is eliminated since it is directly connected with supporting structure;
- * The backup structure is supported by more than two points and these points are *symmetrically spaced so the dish's astigmatism is minimum*;
- * Moment of inertia of the moving parts is smaller than that of Cassegrain design;
- * Smaller back focus distance results in a smaller secondary mirror diameter;
- * A stable and accessible location is provided for sophisticated receiver instruments.
- * It has a smaller sweeping volume, so the baseline between antennas can be minimum;
- * Wind induced pointing error is greatly reduced since maximum wind force is applied to the slant bearing, not the driving gear chain;
- * Lower overall weight will reduce the total cost of the antenna.

2.4 Disadvantages of slanted-axis design

The slanted-axis design has a higher stiffness and other advantages. However, it also suffers from the following disadvantages:

- * The coordinate system is more complicated than that of an altazimuth or polar system; In some direction, the slanted axis antenna needs to travel longer arcs in its two axes than those required in an altazimuth antenna;

- * The deflection of the structure is more complicated than for the Cassegrain design and the bearing induced pointing errors are increased, although most of these errors are correctable;

- * The slanted bearing which is large in diameter is more expensive than small size elevation bearing for other concepts;

- * Since the radiation wave has to pass through the slanted axis, it is very difficult, or impossible, to accommodate an on-axis encoder for it; an alternative way has to be worked out;

- * Wind force applied to the antenna is more complicated since the dish surface is moving along an inclined circular route instead of an in-plane arc route as for an altazimuth mounting antenna.

3. GENERAL DESIGN OF A SLANTED-AXIS ANTENNA

3.1 Antenna arrangement

General views of the proposed slanted-axis MMA antenna are shown in Fig. 1 and 2. This design is not fully optimized. Further improvement of the structure is necessary and possible. However, this preliminary design does give a clear picture of the final antenna and also the parameters of its potential static and dynamic performance.

The whole antenna structure designed can be divided into four parts: (1) The dish and secondary mirror, (2) The slanted-axis and dish support structure, (3) The azimuth bearing and the receiver cabin and (4) The base structure. The structural aspects of these four parts are discussed in detail on this report. Weight comparison between the proposed design and Cassegrain or bent-Nasymth designs is also provided.

The antenna dish structure is an open space truss design mainly built of CFRP material. It has no central hub. 84 panels are supported in four rings on the top of the dish. Each panel is supported on three points. The tripod which supports the secondary mirror is separated from the backup structure. The tripod has a truss type design which is similar to an optical telescope tube^[10]. Both tripod and backup structure are supported by a strong triangle frame which is supported by a shell like truss supporting structure above the slant

bearing. The joints of the supporting structure are soft compared to the main triangle frame so that the change of the supporting force will not affect the surface accuracy of the backup structure. Under the shell like supporting structure, are a strong turntable and drive mechanism. At the other side of the slant bearing, there is a large cabin space for receiver and other related instrumentation. The space within the cabin is more than one cubic meter. The cabin itself is a box type rigid structure. On the base of the cabin, the azimuth bearing and drive mechanism are located. The base structure under the azimuth bearing is a stiff cylinder plate structure. It holds the cable wrap and the attachments for antenna transportation and re-position mechanism.

The total weight of the antenna is estimated at 32 tonnes, including drives and other mechanism needed. It also includes a certain weight of receiver instrumentation. The breakdown of the antenna weight is listed below. The antenna height is 11 m. The slant axis intersects the reflector axis at 1 m below the parabola vertex. The center of the slant bearing is 1.5 m from the axes intersection point. The azimuth axis is 1.2 m away from the reflector axis when it is pointing to zenith. The height of the base is about 1.7 m. The calculated natural frequency of the present model (the analysis model has a weight of 21,000 kg only) is 9.72 Hz; this model includes all the weight of surface panels. The backup structure of this antenna model is not fully optimized. The gravitational rms error from a best fit parabola is 8 μm at zenith pointing and 6 μm at horizon pointing.

3.2 Preliminary weight distribution

Table 1 is a breakdown of the structure weight estimation. In this table, the coordinates of the center of gravity for each related component are also listed. The coordinate origin used is at the vertex of the reflecting surface, the unit used is meters.

Table 1 Breakdown of antenna structural weight

| COMPONENT NAME | WEIGHT | CENTER OF GRAVITY |
|--|----------|-------------------|
| <u>Dish and secondary mirror</u> | 5,600 kg | (0, -0.31) |
| <u>Dish and main frame</u> | 4,200 kg | (0, -0.73) |
| Panels 20 kg/m ² * | 1,100 kg | (0, 0.64) |
| Surface nodes ~ 8 kg/unit | 780 kg | (0, 0.57) |

| | | |
|--|--|---------------|
| Back nodes | ~ 8 kg/unit for outer ring ~ 18 kg/unit for main support ring | |
| | 520 kg | (0, -0.47) |
| Surface beam | 70 kg | (0, 0.59) |
| Middle beam | 110 kg | (0, -0.10) |
| Back beam | 100 kg | (0, -0.47) |
| Bottom beam | 320 kg | (0, -1.65) |
| Main triangle frame | 1,100 kg | (0, -1.10) |
| <u>Secondary assembly</u> | 900 kg | (0, 1.63) |
| Secondary mirror part | 110 kg | (0, 3.40) |
| Secondary support | 1290 kg | (0, 1.38) |
| <u>Dish support structure</u> | 2,100 kg | (0.48, -2.57) |
| <i>structure above slant bearing</i> | 7,200 kg | (0.14, -0.97) |
| <u>Receiver cabin and turntable</u> | 6,800 kg | (2.10, -2.80) |
| <i>structure above azimuth bearing</i> | 14,000 kg | (1.10, -1.86) |
| <u>Base structure</u> | 10,000 kg | (1.14, -2.7) |
| <u>Drive system</u> | 5,000 kg | |
| <u>Receiver instrumentation</u> | 2,500 kg | |
| Total weight estimated | 32,000 kg | |

* The weight used is based on cast aluminium panels.

3.3 Panel design

Millimeter and sub-millimeter antenna panels have been made with different materials and by different manufacturing methods. These include machined cast aluminum with ribs (BIMA panels); aluminum skin with aluminum ribs epoxied on the rear (ESSCO and AT panels); aluminum honeycomb with aluminum facings (thin facings as JCMT panels and thick facings as Caltech panels of which the facings have to be machined); aluminum honeycomb with CFRP facings (SMT panels) and CFRP honeycomb with CFRP facings. Besides panels with a machined aluminum surface, all the rest are made by replicating the surface shape from accurately manufactured molds. The task of the MMA antenna panel design is to choose one or more candidates which carefully fulfill MMA antenna requirements. These requirements include consideration of panel weight, panel surface accuracy, thermal behavior, reflectivity in the visible and infrared, stability under wind and other environmental conditions and cost.

Considering only the weight, machined aluminum panels are the worst choice among all the various possibilities, the typical weight of a cast aluminum panel is 20-30 kg/m². An aluminum skin panel with aluminum ribs is less, about 8-10 kg/m² (note, this is the figure for the NRAO 12-m panels which have a lower surface accuracy compared with others mentioned here). An aluminum honeycomb panel has a weight of about 12-15 kg/m². The CFRP honeycomb panels are lightest of all, about 8 kg/m². One can see, from Table 1, that the center of gravity of surface panels for an 8 m dish is 0.64 meters above the vertex of the parabola, far away from the supporting structure and the antenna rotating axis. Reducing the weight of the panels will be very important in improving the natural frequency and the dynamic performance of the structure.

Considering surface accuracy, the aluminum skin panel with aluminum ribs may have difficulties in meeting the tight MMA specification due to the rebounding effect during the panel's manufacture. All of the other types of panels could be made to specification either by fine cutting or by using accurately made molds, possibly Pyrex.

The thermal behavior of the panels is the most constraining limitation in the design of MMA surface panels. In particular, MMA antennas are required to operate in direct sun light which has a thermal flux of 1.2 kW / m². Delannoy^[13] and Lamb^[12] have discussed this issue in detail. The data provided in this part are based on their work. The thermal effects of the antenna panel can be divided into an absolute temperature (T) effect, and the thermal gradient (ΔT) effect. T effect can be removed by using the same material for the panel and backup structure or by designing a special panel support mechanism. Without these measures, taking d_p as the panel's linear dimension in meters and a 30 degrees variation away from setting temperature, then for the CFRP backup structure and aluminum panels, the rms surface error is:

$$\varepsilon = 7 d_p^2 \mu\text{m}$$

For a steel backup structure and aluminum panels, the rms surface error is:

$$\varepsilon = 2.5 d_p^2 \mu\text{m}$$

For a steel backup structure and aluminum panels, if the variation away from the setting temperature is only 10 degrees, then the rms surface error is:

$$\varepsilon = 2.3 d_p^2 \mu\text{m}$$

In the analysis of the ΔT effect, panel thickness is irrelevant. Instead ΔT effect is related to the material property α/κ of the panel, the thermal flux applied to it and a shape factor m , where α is thermal expansion coefficient and κ is thermal conductivity. Typical values of α/κ are $1.5 \times 10^{-7} \text{ m}^{-1}$ for aluminum and $0.12 \times 10^{-7} \text{ m}^{-1}$ for CFRP. The shape factor for a uniform panel is unity. However, when the ribs are applied to the rear surface, the convective dissipation on the rear surface could increase with a corresponding gradient increase; the factor m would be larger but not more than 2. For a honeycomb structure, the factor m is related to the filling ratio of the honeycomb, expressed as an inverse filling factor which ranges from 10 to 80.

For typical conditions of a one meter square panel subject to one solar flux (the solar emissivity is 0.3, the infrared emissivity is 0.08 and the thermal flux through the panel is 140 W / m^2), a cast ribbed aluminum panel will have a ΔT effect less than $3 \mu\text{m}$; an aluminum honeycomb panel will have a ΔT effect of $15\text{-}120 \mu\text{m}$, and a CFRP honeycomb panel will have a ΔT effect ranging from 0 to $180 \mu\text{m}$, depending upon the true thermal expansion coefficient of the CFRP. The ideal situation would be to use CFRP panels with a thermal expansion coefficient near zero. A CFRP panel with aluminum honeycomb may have an α/κ factor of $2.9 \times 10^{-8} \text{ m}^{-1}$, the corresponding ΔT effect is about $3\text{-}24 \mu\text{m}$.

Analysis of the ΔT effect ruled out the possibility of using an aluminum skin panel with ribs epoxied on its rear surface. This is because this panel has a comparably thick layer of epoxy material which has a thermal conductivity one thousand time less than that of aluminum. For reducing the ΔT effect of other type of panels, one could increase the reflectivity of the panel to reduce the thermal flux through the panels. However a higher reflectivity of panels will remove much of the energy toward the secondary mirror and the receiver. This is undesirable for solar observations. One way to solve this problem will be discussed later.

In summary, the T effect of any panel is usually small ($< 5 \mu\text{m}$) if the size of the panel is not larger than 1 m^2 and the temperature variation is less than 20 degrees. But the ΔT effect is really serious if a honeycomb panel is applied. One could use a cast aluminum panel or a CFRP honeycomb panel with its thermal coefficient adjusted to zero.

As mentioned above, the reflectivity in the visible and infrared places limitations on solar observations. However, reducing the reflectivity of the panels will cause a high ΔT effect, which is also undesirable. One way to overcome this problem is to form a grating-like surface with an inclined angle. This has been done on the BIMA antennas. In this way, harmful and unwanted infrared and visible light will be reflected away, but the useful millimeter wave radiation will be focused to the receiver. This surface could be easily produced on a cast aluminum panel and may be possible to replicate by a specially manufactured mold.

A panel's surface error under windy conditions is predictable and could be reduced by using more ribs or a smaller honeycomb size. However, study of panel stability under environmental conditions shows that some CFRP panels have a significant surface degradation after year around exposure to the environment. Increasing the thickness of the surface aluminum layer would be helpful in reducing this effect. Further tests are still needed to determine this environmental effect.

The above analysis suggests that a cast aluminum ribbed panel with grating-like surface is best. This type of panel can be used under severe thermal conditions and will make direct solar observation possible. Proper processing of the panels has to be provided in order to reduce the time aging wrapping effect. The panel should be about 5-7 mm in thickness with ribs about 100 mm in height. By applying a computer controlled machining technique, the cost could be reduced if a large number of panels is ordered. The penalty of using this type of panel is the weight which is heaviest among all the candidates. The other choice may be a CFRP honeycomb panel with an almost zero thermal expansion coefficient. The weight advantage of this panel is obvious. However, a detailed study of it is required.

The panel size of the antenna is also limited mainly by the thermal effect. The size of each panel should be less than 1 square meter. This applies to all fan-shaped surface panels. Therefore an adequate panel arrangement should be 4 rings, 84 panels for an 8 m antenna. The panel arrangement for the MMA antennas is shown in Fig. 3. The detailed data for the panel are in Table 2. A hexagonal panel shape is also considered. However, three disadvantages become apparent. These are: the outline of the antenna will not be a circle, the surface shape of all the panels within each ring will not be identical and the backup structure design will be more complicated. These considerations make hexagonal shaped panels less attractive.

Many millimeter and sub-millimeter panels are supported at four corner points. Four-point support of a panel is an over constrained system. The unknown constrained force could deform the panels' surface shape. By special design, a three-point support system will result in a stable and determinate panel shape. It will be less sensitive when the panel and backup structure have a different thermal expansion. Furthermore, a three-point support system reduces the number of the surface nodes of the backup structure greatly (from

108 to 96). This will reduce the dish weight considerably since the CFRP tube is light compared with steel or invar node joints. Therefore in this design, all panels are supported by three points. The panel arrangement and the their support points are show in Fig. 3. The radius and height of the third support points of the panels are also listed in Table 2.

Table 2 Panel geometry and related data

| | ring 1 | ring 2 | ring 3 | ring 4 | total |
|-------------------------------|---------|--------|--------|--------|--------|
| number per ring | 12 | 24 | 24 | 24 | 84 |
| x coordinate inner radius | 0.3 | 1.35 | 2.45 | 3.3 | |
| x coordinate outer radius | 1.35 | 2.45 | 3.3 | 4.0 | |
| y coordinate inner edge | 0.00731 | 0.142 | 0.469 | 0.851 | |
| y coordinate outer edge | 0.142 | 0.469 | 0.851 | 1.25 | |
| radial length | 1.0598 | 1.1486 | 0.9322 | 0.8058 | 3.946 |
| longest arc length | 0.706 | 0.641 | 0.864 | 1.047 | |
| panel area | 0.4565 | 0.5733 | 0.7028 | 0.782 | 54.893 |
| third support x coordinate | | 2.0 | 2.95 | 3.7 | |
| third support y coordinate | | 0.312 | 0.680 | 1.068 | |

* units in Table 2 are meters and square meters.

3.4 Backup structure design

Among existing antenna backup structures, a box-type central hub design is popular. This type of design makes it easy to achieve a homologically deformed surface pattern. The strong box-type central hub distributes supporting forces symmetrically and evenly around members of the backup structure. These supporting forces of the backup structure are usually unsymmetrical axially either from elevation bearings or from the drive mechanism. However, a strong central hub brings more weight to the backup structure, typically 1,000 kg for an eight meters antenna dish. This additional weight makes the response of the antenna slower. Furthermore, mass at the central hub causes a larger thermal time constant than those of the rest of the backup structure. In this way, the temperature gradient will be large within the structure when the environment temperature is changed. This is undesirable for the MMA antenna.

Another feature of some antenna designs is to employ only radially in-plane truss structure. These in-plane trusses are supported by a central hub acting like cantilever beams. This feature of design also makes it be easy to reduce the residue node deflections after a best fit parabola is applied, since every member's change of the trusses will only affect the displacement along the plane where the member is located. However an in-plane truss design is always less efficient than a space truss design if rigidity is required in more directions. In the same time, a cantilever type design is also less stiff and may result in larger displacements and member stresses.

For achieving a rigid, thermally stable backup structure design, a JCMT type backup structure which was developed from the MaxPlanck 100-m design is adapted in the proposed MMA antenna. The basic geometry of this design is to form a symmetrical space structure by connecting it from two on-axis points, the front point is a small central ring of the backup structure and the back point has a ring of projected members which support the backup structure on the middle from its back side. The back on-axis point takes most of the load of the dish when it points to zenith or faces to strong wind. Both front small ring and back on-axis point are then supported by a strong triangle main frame. Figure A2 shows the core of the backup structure and the triangle frame. The front ring supporting truss from the main triangle frame is a Serrurier type truss which has a high torsional stiffness as discussed in the Appendix. Since the designed backup structure is supported not only from its center ring, but also from a larger radius by twelve projected beams from the back on-axis point, the absolute deflections and member stresses will be small. This arrangement and space truss design make it be possible to form most of the backup structure by only few member cross-section areas. In the present design, most of members forming the space trusses have a uniform cross-section area. However, optimization of the structure deflection pattern without changing the member cross-section areas does take time.

As mentioned in the previous section, it is necessary to reduce the number of the joint

nodes. These nodes for connecting CFRP members are heavy in weight. The number of back side nodes of the structure is also optimized. The total node number for the backup structure is only 156. The backup structure geometry and triangle main frame is shown in Fig. 4.

This design achieves a rigid, light weight, thermally desirable backup structure, although the final target of 5 μm rms gravitation error is still not fulfilled. It is very likely to achieve this by further modification. At present, the best results obtained are 8 μm for zenith pointing and 6 μm for horizon pointing.

3.5 Secondary mirror support design

Traditionally, antenna secondary mirrors have been supported by straight tetrapod or tripod structures. These structures are stiff in both axial and radial directions but they present no rotational stiffness if the model is a pin-jointed one. By splitting the supporting legs of a tripod structure and adapting a design which is similar to the optical telescope trusses, the torsional stiffness is then increased. This structure is the secondary mirror support structure adapted by this design. It is developed from the JCMT design^[11], which uses a four-side eight member trusses to support its secondary mirror. In the Appendix, discuss has been made on the torsional stiffness between this type trusses with different number of sides. The three-side six member structure has been proved to be the best on torsional stiffness. However, this type of secondary support has a complex blockage pattern and demands a larger leg bottom radius (the radius where the supporting leg intersects the reflecting surface) to reduce its indirect blockage. This makes the structure be less stiff.

In this design, another feature of the secondary mirror support structure is that it is connected directly to the strong triangle main frame which also supports the backup structure. It is therefore separated from the backup structure itself. This avoids undesirable deformation of the backup structure shape caused by the weight of secondary mirror and its supporting structure. However, this arrangement makes the tripod designed be not very stiff, since the distance between secondary mirror and the triangle main frame is large. In the beginning of the design, the structure is weak, its natural frequency is only 8 Hz. After adding members at the bottom part of the structure, the natural frequency of the structure has been improved to 12.59 Hz. In the design, the weight of secondary mirror part assumed is 100 kg. However, this design still results in larger pointing error when the wind is strong. Further improvement of this structure will be made in order to stiffen the supporting structure.

At this moment, all the supporting members below the panel surface are made from steel tube, and above the panel surface are made from CFRP. By considering thermal effects of the secondary mirror position, it may be helpful to use CFRP in all the tripod structure. The results of this change are that the weight is reduced and the natural frequency is reduced

as well(because the Young's modulus of CFRP is less than that of steel).

During the tripod design stage, the traditional three member tripod and the 6 member tripod have been compared by running NASTRAN analysis. With the same structural weight and the same support condition, the natural frequency of the latter one is 4 times bigger than that of the former one, and the lateral stiffness is also improved. The two analysis models are shown in Fig. 5. The first traditional model has member size of 10x100 mm and the weight of the secondary mirror is 200 kg. The natural frequency calculated is 11.4 Hz. In the second model, only six beams 7 to 12 have their cross-section size of 5x100 mm and the rest of the beams remain unchanged, then the natural frequency becomes 48.9 Hz. Under gravitation, the top end deflections of the former one are 0.82 mm and 3.52 mm for zenith and horizon pointings respectively. Those of the latter one are 0.10 mm and 0.10 mm.

3.6 Slanted-axis structure design

The slanted-axis structure includes a slant bearing turntable and a shell like supporting truss structure for the antenna dish. The turntable, including bearing, drive and encoder system, should be comparably strong to allow a fast movement around the slant axis. The bearing required is a 2.5 meter diameter heavy load bearing. The supporting truss structure surrounds the bottom part of the backup structure and determines the position of the triangle main frame of the backup structure. It is very stiff in transferring the torsional moment of the reflecting dish to the drive turntable. If necessary, a thin membrane can be added to the truss structure to further stiffen the supporting structure. Inside the slant bearing, a mirror, the fourth mirror of the antenna, is located to direct the radiation to the receiver.

The connections between dish triangle frame and the supporting trusses are critical and need more attention to ensure that they have little effect on the backup structure shape when the dish is in different pointing directions. Details of this connection are still not drawn out, but a slightly soft joint might allow the distortion from the variable supporting force not to affect the strong triangle frame.

3.7 Receiver cabin design

The receiver cabin is a strong box structure made with steel trusses and surface plates. The box structure supports the slant bearing turntable. It will houses the receiver instruments and some balance weight. Outside the box, insulation is necessary to keep the structure at a uniform desirable temperature. In the preliminary structure analysis, the plate elements have not been added for the receiver cabin. On the bottom of of the receiver cabin there is the azimuth turntable which could be made identical to the slant bearing turntable.

3.8 Antenna base design

The antenna base is a strong tank shaped structure. The bottom of the base structure is a stiff triangle base frame. The antenna positioning device is located on the base frame. The main cable wrap is inside the base structure. The base is fully insulated to reduce pointing error. The base structure also houses the transportation attachment. For reducing thermally induced pointing error, a tilt meter can be used on the top of the base structure.

3.9 Drive and encoder consideration

3.9.1 Secondary mirror drive

The secondary mirror should allow movement with five degrees of freedom in order to compensate displacements in all these directions. In this way, pointing errors caused by gravitation and thermal gradients between six truss legs can be corrected. These five degrees of freedom are all three linear movements and two rotating movements. The two rotational movements are at the directions which are perpendicular to the mirror axis. The calculated linear displacements under gravitation are within 2 mm range and the tilt is within 3 arc min range. Gravitational compensation is straightforward. Thermal and wind(partly) displacement compensation could also be made in the future.

3.9.2 Turntable drive

Turntable drive, either slant axis or azimuth axis ones, can be designed by using an anti-backlash spur gear system. However, this demands a very accurate drive gear pair which is very expensive. On the other hand, the friction roller drive system has been proved to be reliable, inexpensive and free from backlash. It has been applied at a number of large telescope projects, and it can be used for the future MMA antennas.

The friction drive system is formed by two drive rollers. The drive rollers are simply in geometry and can be made accurately in shape. The drive force is transferred by friction force which is proportional to the contacting pressure between two rollers. By adjusting the contacting pressure the force it transfers could be determined accurately. In practice, slippage can be avoid and the drive force can be servo controlled to take care of the low frequency part of the outside disturbance. At this stage, no detailed calculation has been made for either the slant axis or azimuth axis drive systems. However, it is possible to design the drive system and to overcome the disturbance from wind force. For transferring large drive loads, the roller surface has to be hardened to sustain maximum surface stress. The maximum contacting stress of a pair drive rollers are(if the Poison's ratio of the material is 0.3):

$$\rho_{\max} = 0.418 [(PE((1/r_1)-(1/r_2)))/L]$$

where P is the contacting pressure, E is young's modulus, r_1 and r_2 are radii of the rollers and L is the contacting length.

For the slanted-axis design, the disturbance of the drive force is not the same as that of an altazimuth mounting system. Detailed study is needed in determining quantitatively the wind induced drive force in both slanted axis and azimuth axis. Another advantage by applying a friction drive system is that the accuracy and stiffness of drive turntable could be improved. In the proposed design, a commercial heavy load bearing is used. However, these bearing have limited stiffness and accuracy. If the main drive disk is accurately manufactured and the drive rollers are properly preloaded, then the accuracy of turntable is determined by the drive rollers. And the stiffness of whole turntable is the sum of the stiffnesses of the bearing and the drive rollers. In this way, the accuracy required of the bearings may be reduced to allow a slightly large runout. The same surface of the drive disk(not the same portion) also can be used for encoder system.

3.9.3 Encoder system

The encoders used at both axes include absolute and incremental ones. The purpose of the absolute encoder is to provide a zero point for calibration and that of incremental encoder will ensure the 1 arc sec pointing requirement. The absolute encoder can be a coarse one. One kind of magnetic switch(made by Sony Co., USA) has a position repeatability of 1 micron(it corresponds to 0.2 arc sec if it is used on a disk of 2.5 m diameter). It can serve as an absolute encoder if these switches are placed every 15 degrees or less on the main drive disk, or a coarse grating tape can be used for this purpose. The incremental encoder should have 17 to 19 bit accuracy. The incremental encoder is coupled to the main drive disk. The coupling ratio for the incremental encoder is such that each increment corresponds to 0.1 arc sec of antenna axis rotation. Each encoder is interfaced to a real time microprocessor controller. Using the incremental encoder as an interpolater between absolute encoder transitions, which repeats to about 0.2 arc sec, the system will have 0.2 arc sec accuracy over large angles and higher relative accuracy over smaller angles.

4. DYNAMIC ANALYSIS OF THE STRUCTURE

4.1 NASTRAN model

The antenna model used for the NASTRAN analysis involves the following elements: CBEAM, CELAS2, CONM2, CTRA3, CQUAD4 and RBE2. CBEAM elements are elements commonly used in truss structure, as are the plate elements like CTRA3 and

CQUAD4, but the surface panels used during analysis are modeled as thin plates with aluminium mass density but a very low Young's modulus. This simulates the case where panels apply weight to the backup structure but do not provide stiffness to it. The joint node mass in the backup structure and other additional masses are represented by concentrated mass elements CONM2. The model for bearing parts is complicated. In the model, two sets of grids, each set comprising 12 grids evenly distributed at the same radius, are defined with an identical coordinate value. These two sets of grids are connected by 48 members. Among these 48 members, 24 members are beam elements which connect grids within each set, and 24 are elastic members which connect corresponding grids between sets. These two sets of spring elements, called as CELAS2, represent radial and axial elastic connections between the pair of grids respectively. The spring constant used are from existing bearing catalog data. To simulate the elastic property of the drive system, one additional pair of grids is used. These two grids also have identical coordinate values and they are connected to the nearby pair of grids on the bearing rings by two rigid beams element RBE2. Between these two grids, another elastic CELAS2 element with a spring constant in the tangential direction is used to represent the elasticity of the drive pair. The stiffness data used for these drive spring elements are also from the manufacturer. Table 3 lists the bearing axial and radial stiffness of a 2 m diameter cross roller bearing. By considering all these special elements, the analysis model developed is reliable.

Table 3 Stiffness of 2 m Rotex grade G0 cross-roller bearing

| | |
|------------------|------------------------|
| axial stiffness | 1.5735e+9 N / m |
| moment stiffness | 7.0233e+9 N-m / radian |
| radial stiffness | 8.2470e+8 N / m |

4.2 Loadings for analysis

In the NASTRAN analysis, three simplified loading conditions have been used. These are the gravitation loading only, gravitation loading plus working wind loading and gravitation loading plus survival condition loading. The survival loading includes wind force, and ice and snow loading. Some of these loadings are calculated here. Other loading models are complex and it will produced in the future running.

Wind loading is important for antenna analysis. Wind pressure is expressed as:

$$P = C_d * \rho * v^2 / 2$$

where ρ is air density, at sea level, $\rho = 1.226 \text{ kg/m}^3$. at 3,000 m level $\rho = 0.819 \text{ kg/m}^3$, C_d is a shape factor $C_d \sim 2.0$ for a concave surface; for other shapes, it will be smaller. Under working conditions the maximum wind pressure on the panel surface is:

$$P_{\text{work}} = 511 \text{ N/m}^2 \quad V = 25 \text{ m/s}$$

At survival condition the wind pressure on the panel surface is:

$$P_{\text{sur}} = 2950 \text{ N/m}^2 \quad V = 60 \text{ m/s}$$

Total wind force during survival condition on the dish is:

$$W_{\text{wind}} = 1.6 \times 10^5 \text{ N} \quad \text{the aperture area of the antenna is } 50.2 \text{ m}^2$$

For secondary mirror, take $C_d = 1.5$, then

$$P_{\text{sur}} = 2.2 \times 10^3 \text{ N/m}^2 \quad P_{\text{work}} = 384 \text{ N/m}^2$$

Total force during survival condition on secondary mirror is:

$$W_{\text{sec}} = 1104 \text{ N} \quad \text{the projected area of secondary mirror is } 0.5 \text{ m}^2$$

Ice and snow pressure and loading:

For parabolic surface of revolution, if the surface equation is:

$$X^2 + Y^2 = 4 a Z$$

then the surface area S is:

$$S = (8\pi/3) (a^{(1/2)}) [(Z_1 + a)^{(3/2)} + (Z_2 + a)^{(3/2)}]$$

for MMA dish, total panel surface is $S = 55 \text{ m}^2$

Maximum ice pressure on panel surface is $P_{\text{ice}} = 894 \text{ N/m}^2$

So maximum ice loading on whole dish will be $W_{\text{ice}} = 4.9 \times 10^4 \text{ N}$

And the maximum snow loading on whole dish is $W_{\text{snow}} = 4.4 \times 10^4 \text{ N}$

Since both snow and wind loading will not be applied to the dish at the same time only the wind plus ice loading is taken as the extreme survival loading on the dish surface. The extreme pressure on the panels is $P_{\text{extr}} = 3840 \text{ N/m}^2$ and the total survival loading on the dish is $W_{\text{extr}} = 2.1 \times 10^5 \text{ N}$. These surviving data are used for checking the structure stress condition of the antenna.

4.3 NASTRAN dynamic analysis results of the design

NASTRAN dynamic analysis has been performed for parts of the preliminary design. These parts are the backup structure, the tripod structure, parts which combine both the above two parts, parts above the slant bearing, parts above azimuth bearing and parts of all the antenna structure. In the first part of the analysis, the weight of the surface panels are not considered. In the end, the weight of surface panels is added to get a real data for the natural frequency. In the process of the analysis, the structure has been improved gradually. In the following table, natural frequencies of different models are listed. In the table, the net structure weight is also recorded for reference. This net weight does not include some detailed mechanisms like drive or cablewrap systems.

Table 4 The results of antenna dynamic analysis

| part name | model number | frequency | net weight |
|------------------|--------------|-----------|------------|
| Backup structure | part1-01 | 6.6 Hz | 2790 kg |
| | part1-02 | 12.5 | 2795 |
| | part1-03 | 13.1 | 2801 |
| | part1-04 | 13.2 | 2804 |
| ---- | dish | 15.9 | 2780 |
| tripod and frame | part2-01 | 8.7 | 1600 |
| | part2-02 | 12.4 | 1650 |

| | | | |
|-------------------------|-----------------------|-------|-------|
| | part2-03 | 12.5 | 1680 |
| ---- | tirp | 12.6 | 1650 |
| dish as a whole | part12-01 | 12.5 | 4439 |
| ---- | distp | 12.6 | 4440 |
| ---- | distp with panel | 12.1 | 5280 |
| part above slant axis | part123-01 | 11.6 | 6900 |
| | part123-02 | 12.1 | 6625 |
| part above azimuth axis | part1234-01 | 10.6 | 11320 |
| all part | partall-01 | 9.9 | 16100 |
| ---- | v01 | 11.2 | 20370 |
| ---- | v02 | 11.2 | 20410 |
| ---- | v03 | 11.2 | 20450 |
| ---- | v04 | 11.37 | 20510 |
| ---- | v05 with panel weight | 9.72 | 21360 |

Figs. 5 and 9 show models of the antenna dish and antenna structure. Figs. 6 to 8 show the vibration modes of the dish structure and Fig. 10 shows the first mode of vibration of the MMA antenna structure.

4.4 Comparison with Cassegrain and bent-Nasymth design

In this paragraph, a comparison on the weight and natural frequency of three types of antenna structures is provided. These three types of structures are Cassegrain structure, bent-Nasmyth structure and slanted-axis structure. The Cassegrain concept is widely used in the fields of optical and radio telescopes. It has been adapted by the 6m BIMA antennas for a millimeter array. The bent-Nasmyth concept has been recently developed for the 6 m SMA antennas, also for a millimeter array. The arrangements of these two designs are show in Fig. 11 and Fig. 12, both of them are good for millimeter wavelength antennas.

From azimuth turntable downwards, all these three designs are similar to each other if the mass difference of them is ignored. If the moments of inertia about azimuth axis are considered, the slanted-axis design would have a larger moment of inertia when the dish is pointing to zenith. This is because the dish is offset from the azimuth axis in this design. However, when the antenna is pointing to horizon, the moment of inertia of all three concepts will be similar since the dishes are all on one side of their azimuth axes.

However, from azimuth turntable upwards, all these three designs are totally different. In the Cassegrain and bent-Nasmyth designs, fork structures are provided on the top of azimuth turntables. For the Cassegrain design, countweight, elevation drive and receiver cabin are all located between two fork arms. The opening of the fork is large and the height of fork arms is long. This arrangement produces a symmetrical force condition on the azimuth bearing but it makes the structure heavier and less stiff. For the bent-Nasmyth design, two fork arms are close to each other and the receiver cabin is located behind these fork arms. This arrangement is compact and fairly rigid but it produces an unsymmetrical force condition when the dish is pointing to zenith. For slanted-axis design, a box type receiver cabin is located on the top of the azimuth turntable. The receiver cabin is rigid and compact. The weight of the cabin is also balanced by the dish structure, so the force condition on the azimuth turntable is also symmetrical. Up to this point, the slanted-axis design is superior over the other two designs in both rigidity and force condition. Further up to the second axis, it is also possible to make a comparison. For the Cassegrain design, the elevation axis is on the top of the fork arms. The dish is supported by the elevation bearings via a rigid box type frame. The dish weight is balanced by the receiver cabin and countweight. The weight and moment on the elevation axis is very big. But the force condition on the axis is still symmetrical. For the bent-Nasymth design, the dish is not balanced and a drive screw is used to push the dish. The drive force varies both in direction and magnitude when the dish is moving around the elevation axis. Therefore it requires a strong supporting structure for the dish. But the weight and moment on the axis is much smaller than those of the Cassegrain design. For the slanted-axis design, the slanted turntable is on the side of the receiver cabin. The dish is directly supported by a shell like truss structure which is rigid and there is no countweight on the back of the dish. The force applied to the bearing is not symmetrical but is stationary as the axis passing through the center of gravity of the rotating parts. Therefore, the slanted-axis design still results in a rigid and light weight structure compared with the Cassegrain and bent-Nasmyth design.

Another advantage of the slanted-axis design is that it will have less effect of pointing error by the wind. But the unsymmetrical arrangement will cause some unbalanced problem on the slanted axis. The weight distribution of these three designs is estimated and listed in Table 5. In this table, the weight of the backup structure is taken as unit.

Table 5 Weight estimation of different design concepts

| | Slanted-axis | bent-Nasmyth | Cassegrain |
|-----------------------|--------------|--------------|------------|
| Backup structure | 1 | 1 | 1 |
| dish support part | 0.2 | 0.4 | 0.4 |
| dish counterweight | 0 | 0 | 0.5 |
| receiver cabin | 1 | 1 | 0.4 |
| fork or slant bearing | 1 | 1 | 1.6 |
| base structure | 2 | 2 | 2.5 |
| total weight | 5.2 | 5.4 | 6.5 |

The natural frequency of the antenna structure is an important parameter. The natural frequency is directly related to the stiffness and the mass of the structure. The weakest point of a structure usually determines the lowest natural frequency of the whole structure. In any antenna design, the weakest point is usually the dish support structure. The dish is supported by only two points for any altazimuth antenna structure, The tall fork arm causes the first few modes of the vibration(see Fig. 13) of the antenna structure[14]. Sometimes, the torsion mode is more interesting to the designers since the azimuth drive moment can excite vibration in this direction easily. The formula of the torsional natural frequency for an elevation mounting structure is:

$$v = (\pi/2)(EI/(Mr)*(L^4))^{(1/2)}$$

where M is the moment of inertia of the dish, L is the length of fork arms, and I is the moment of inertia of the arm section. The Cassegrain design has a larger L , because of the receiver space behind the dish. However when L is large, the natural frequency of the structure will be low. By increasing r , the distance from the fork arm to the dish axis, or by increasing I of the arm section the effect of L can be reduced. However, this increases the structure weight, which, in turn, affects the stiffness of the antenna. Classical Nasmyth designs can have a very short L resulting in a higher stiffness of the structure. But if the receiver cabin is located outside the the elevation bearings, the moment of inertia of the structure about the azimuth axis will be larger.

For the bent-Nasmyth design, the previous formula is also applied. Here L is not short as the receiver cabin is vertically in front of the fork arms. But the fork arms of this design are connected with the box-type cabin. This makes the fork structure more rigid. However, the weakest part of this design is the driving screw, which is long and slender. When the screw is at a position where the length of it is longest, the formula of the structural frequency due to the bending of the screw caused by the moment of inertia of the dish is:

$$v = (1/2\pi)(EA/(L*(M/d)))^{(1/2)}$$

where d is the distance of the screw to the altitude bearing, A is the area of the drive screw, L is the effective length of the screw. Since A is very small, d is small and M and L are large, the natural frequency is low. When the dish is away from the zenith, the screw is under compression force. It has a lateral vibration mode. The formula of the natural frequency in this mode is as:

$$v = [1-(M/d)*L^2/(E*I*\pi^2)](\pi/2)(EI/\rho*A*L^4)^{(1/2)}$$

where ρ is the density of the screw, A and I are area and moment of the screw. In this formula the later part is the frequency of the screw without an axial dish load, the first part is an amplification factor which could be near to unity if the rod has a larger moment of inertia compared with the length and the moment of the dish.

By comparison, the slanted-axis design has a shell like truss support design. The formula for its torsional natural frequency is:

$$v = (1/2\pi)(GJ/ML)^{(1/2)}$$

where J is the sectional torsion constant of the supporting shell-like structure, which has a diameter much larger than those of the fork arms or a slender drive screw in other designs. And L , the length of the shell like structure, is also short in comparison with the length of

the fork arms of the other options. Therefore the slanted-axis design should have a highest natural frequency if the structure is designed with the same structure mass.

In this preliminary design, since the whole structure is a light weight design and the panel used is the same weight as other designs its natural frequency may be not very high. But if necessary, a higher natural frequency of the structure is achievable.

4.5 Dynamic requirements for fast switching

Fast switching is the most demanding requirement of the MMA antennas; it requires special discussion and study. In this paragraph, only a rough estimation is provided. If the antenna is required to travel back and forth every six seconds, then a reasonable distribution of time would be 1 second to travel back and forth and 5 seconds to observe and to calibrate. To achieve this target, the settling time of the structure should be about 0.5 seconds (half of 1 second). From control theory^[11], the transient response of an under-damped second-order system is:

$$c(t) = 1 - (e^{-\xi\omega t} / (1-\xi^2)^{1/2}) \sin(\omega t + \tan^{-1}((1-\xi^2)^{1/2} / \xi))$$

where ξ is the damping ratio, ω is the natural frequency and t is the time. The response curve from the formula falls on an area enveloped by two curves of $1 + (e^{-\xi\omega t} / (1-\xi^2)^{1/2})$ and $1 - (e^{-\xi\omega t} / (1-\xi^2)^{1/2})$. If we require the system to be constrained to a certain accuracy, the time needed can be estimated from the envelope equations directly.

If an 8-m antenna travels 1.5 degrees (the separation between source and calibrator) and the pointing error is 1 arc sec, then the required accuracy of the response is 1.85×10^{-4} ($1/(360 \times 60 \times 60)$). Taking the setting time as 0.5 sec, for an optimized control system, the damping factor ξ is 0.7, then the required natural frequency of the structure ω can be solved from the formula:

$$- \xi\omega t = \ln(1.85 \times 10^{-4} (1-\xi^2)^{1/2})$$

the calculated ω is 26.4 sec^{-1} which is 4.2 Hz. This means that the antenna drive system can respond to the fast switching even its natural frequency is only 4.2 Hz. Shortening the settling time, required frequency will be higher. For a 0.1 sec response, the frequency required is 20 Hz. From these data, it seems that the antenna structure can be designed to respond to the switching requirement of the drive system which is as fast as 0.2 sec.

Taking the structure, without consideration of the drive system, the damping factor is much lower. Then the required setting time would be more difficult to achieve. At the moment, there are no existing data available on the damping factor of antenna structures; a particular study on this subject is required. The following is only a brief introduction. For

a structure, there are several ways of expressing damping^[15]; one of them is by the Q factor. $Q = 1/(2\xi)$. The structural damping includes inherent damping and added damping. The inherent damping includes material damping and damping in structural joints. The material damping of a steel or aluminum structure is very small; the Q factor is of the order of 1000. For composite materials the damping is an order of magnitude higher. However, due to the damping in structural joints, the Q factor would be different. The Q factor of a typical bolted steel structure is between 20 and 60, for a typical welded steel structure, it is between 30 and 100. For CFRP antenna structures, no data is available, but it is believed that the Q factor should be between 10 and 30. However, it is very difficult to optimise or control this kind of damping. For antenna structure, there may exist some added damping due to the panels and their supports. The added damping acts as a mass spring system called a vibration absorber. If the parameters of the absorber are chosen carefully, the amplitude of the vibration in a particular frequency range can be greatly reduced. For the antenna structure, the panels applied might act as added damping sources. Assuming the damping factor of an antenna structure is 0.1, then the frequency required for a 0.5 sec setting time is 27 Hz. If the damping factor is 0.05, then the frequency required is 54 Hz. These frequencies are not easy to achieve. However, before the structure is finally setted. the antenna vibrates at a high frequency, the positioning error is called jitter error which could be allowed if they are not very big. Therefore we could double the required setting accuracy to 2 arc sec instead of 1 arc sec. Then the frequency required for the structure with a damping factor of 0.1 and a setting time of 0.5 sec is 16.8 Hz. If the damping factor is 0.05 the frequency required is 33.6 Hz. This makes possible to achieve a 0.5 sec setting time if the damping factor is larger than 0.1. From cost point of view, it is not economic to design a structure with very higher natural frequencies.

From the above discussion, the damping ratio of the antenna is an important factor for the fast calibration switching. Higher damping factors help the structure to set at a faster pace and it avoids an excessively rigid design. To achieve a higher damping ratio, CFRP is a desirable material. Improving the panel's supporting rod design is also important. In case if necessary, damping materials may be used in certain places of the structure. A structure with a high damping ratio also resists wind induced vibration or errors. But a higher damping ratio brings hysteresis, which is undesirable, to the structure design and its surface shape.

Fast switching is also restricted by other factors, such as driving torques and acceleration induced deformation of the structure. These aspects also require further study.

5. STATIC GRAVITATION ANALYSIS OF THE STRUCTURE

5.1 Backup structure arrangement

The backup structure used in this design is a complex truss structure. However almost all the beams used are uniform in size. The whole structure can be divided into several sub-

parts. These sub-parts are the front sub-part of the truss, the middle sub-part of the structure, the back sub-part of the structure and the bottom projected sub-part of the structure. The front sub-part has 96 nodes which support four rings of surface panels. The arrangement of beams is shown in Fig. 14. All beam members of the front sub-part are made of 25 mm diameter CFRP tubes. The middle sub-part of the structure is more complicated. The optimization of the structure is main done by adjusting the location and coordinates of the bottom nodes. The middle beam arrangement is shown in Fig. 15. Again all the middle sub-part members are made of the same 25 mm diameter CFRP tubes. The back beam arrangement is simple. The arrangement of the back sub-part and the bottom sub-part is shown in Fig. 16. The bottom sub-part of the structure is 12 projected beams which connect the on-axis bottom node and the back second ring nodes. These members are 76 mm in diameter. They are steel tubes which support almost 80 percent of the weight of the backup structure when the antenna is at the zenith pointing. These members increase the stiffness of the structure greatly. The back sub-part of the structure also uses the same 25 mm diameter CFRP tubes except two inner rings of circumferential members. These circumferential members are made of larger size square tubes. Altogether, the backup structure uses only four different size of beams. This will greatly reduce the cost if the antenna is mass produced.

The 25 mm diameter of CFRP tube used for most of the backup structure is determined by considering an extreme loading case. The case is that only one single beam member supports an entire panel under survival condition, which is unlikely for the antenna. Assuming the panel size is 1 square meter, and the beam length is 1.5 m. The total load applied on the member is wind load, ice load and panel's self weight as:

$$P_{cr} = 4413 + 9.13 + 196 = 4618 \text{ N}$$

The moment of area required of the CFRP beam can be calculated from the beam's buckling condition. The formula is:

$$I = P_{cr} * L^2 / (2 * \pi^2 * E)$$

where $P_{cr} = 4618 \text{ N}$ and $E = 1.27 * 10^{11} \text{ N/m}^2$ for CFRP then:

$$I = 1.301 * 10^{-8} \text{ m}^4$$

For tube size of 25x3 mm² the radius and moments are:

$$R_1 = 0.0125 \text{ m} \quad R_2 = 0.009 \text{ m} \quad I = 1.40 * 10^{-8} \text{ m}^4$$

By considering the loading condition, it is possible to use this size tubes for the main backup structure members. Of course, the stress check of the final design is still important as it is mentioned later in this report.

For determining the size of the bottom 12 projected beams, an extreme case is also considered. In this extreme case all the backup structure loading under a survival condition is supported by only these 12 projected beams. The load supported by these members are extreme wind loading, ice loading and panels' self weight. The load applied to each member is also magnified by a cosine value of the inclined angle (assumed to be 45 degrees). The total loading is:

$$P_{cr} = (226731 + 25000) / (12 * \cos 45) = 29667 \text{ N}$$

Using the same formula as before, take $E = 2.068 \times 10^{11} \text{ N/m}^2$ for steel and $L = 4 \text{ m}$ then

$$I = 3.65 \times 10^{-7} \text{ m}^4$$

Take $E = 1.27 \times 10^{11} \text{ N/m}^2$ for CFRP then

$$I = 5.95 \times 10^{-7} \text{ m}^4$$

For steel tube, if the member size is $64 \times 6.4 \text{ mm}^2$. The area and moment are:

$$A = 1.146 \times 10^{-3} \text{ m}^2 \quad I = 4.731 \times 10^{-7} \text{ m}^4$$

For CFRP, if the member size is $76 \times 6.4 \text{ mm}^2$. The area and moment are:

$$A = 1.34 \times 10^{-3} \text{ m}^2 \quad I = 8.618 \times 10^{-7} \text{ m}^4$$

These member size data can be used for the antenna structure. Again the stress checking is important to ensure the safety of the structure. •

In the first model of the antenna backup structure, some diagonal members between radial lines and rings are missing. The model resulted has a low frequency in the torsional direction. After adding few more members in the structure, the frequency improved significantly. But, optimization of the surface node deflection does take some time.

5.2 Formulas for parabolic surface fitting

After dynamic analysis, the antenna model has been run by NASTRAN program under survival loading condition. The purpose of this analysis is to check the stress level of all members. The results of this stress checking will be presented on Section 5.4. After stress checking, an important step of the antenna design is to optimize its backup structure to ensure that the deflected surface nodes remain on or near to a best fit parabola when the antenna is under gravitational loading at any orientations.

In contrast to an altazimuth antenna, when the slanted-axis antenna rotates around its slant bearing, the gravitational force relative to the backup structure will sweep on a conic shape surface around an inclined axis instead of being on a fixed plane perpendicular to the elevation axis. The gravitational force at the local backup structure coordinate system has components as:

$$\begin{aligned} |g_x| &= |0.5(1 + \cos \theta)| \\ |g_y| &= |0.5(1 - \cos \theta)| \\ |g_z| &= |0.707 \sin \theta| \end{aligned}$$

where θ is the angle on the slant axis. For any structure under the gravitational load, the deflection of the structure can always be decomposed into components in a local coordinate system. Each deflection component represents the deflection of the structure under the related gravitational load component. In this way, if structure deflections under three particular gravitational load conditions along local coordinate axes are known then the deflections at any orientation will be easily predicted by a similar formula:

$$\varepsilon = \begin{bmatrix} 0.5 (1 + \cos \theta) \\ 0.5 (1 - \cos \theta) \\ 0.707 \sin \theta \end{bmatrix} [\varepsilon_x, \varepsilon_y, \varepsilon_z]$$

where ε_x , ε_y and ε_z are deflections when the antenna is under gravitational loadings on x, y and z axis of the local coordinate system.

From the formula of parabolas, if all three deflection patterns ε_x , ε_y and ε_z fit very well with three particular parabolas, then deflection at any slant angle θ will also fit very well with a parabola. The formula of this parabola is the similar as the formula for the deflection calculation. However, in practice, there will be some residues during fitting, then the rms error of the surface nodes away from a best fit parabola at any slant angle will be:

$$H^2 = (0.5 H_1 (1 + \cos \theta))^2 + (0.5 H_2 (1 - \cos \theta))^2 + 0.5 (H_3 \sin \theta)^2$$

where H_1 , H_2 and H_3 are the residual rms errors of the antenna surface from a best fit parabola under gravitational force x, y and z axis. If the backup structure is fully symmetrical, H_2 is equal to H_3 , then the formula takes the same shape as that for the altazimuth mounted antennas. The formula is:

$$H^2 = (H_1 \cos \delta)^2 + (H_2 \sin \delta)^2$$

where H_1 and H_2 are rms error when the antenna is pointing to zenith and horizon. δ is the zenith distance of antenna.

The least square fitting formulas used in this design are derived by choosing displacements of the vertex point, change of the focal length and rotating angles around axes which are perpendicular to the symmetrical axis as variables. The formulae are derived to minimize the distances between each node to the best fit parabola. The difference between minimum distance and minimum wave path is small. The fitting program is a recently rewritten version by the author. In the program a uniform weighting function is used. A graphical package, PVWave, has been used for the residual surface error display.

5.3 Parabolic surface error under gravitation force

Static analysis of the antenna backup structure under gravitational load has been performed by using the NASTRAN program. Since the backup structure is fully symmetric, the deflection patterns for the two horizon pointing cases are the same. The analysis is then

performed both at zenith pointing and one horizon pointing. The reflector surface grid displacements of these two pointing case are obtained from the output of the analysis. For input to the fitting program, both the grid coordinate data and displacement data are extracted from the output file of the NASTRAN run. These data are then input to the fitting program to calculate the parameters of the best fitting parabola. At the same time, the rms deviations of the deformed surface nodes away from the best fit parabola are calculated. These deviations are then input to another program for format conversion of PVWave program. The final results can be displayed as surface map or contour maps.

Table 6 The best fit result of a backup structure model

Case 1 zenith pointing

rms error =8.0 μm

vertex displacement $d_x = 0.504 \times 10^{-9} \text{ m}$ $d_y = 0.241 \times 10^{-9} \text{ m}$ $d_z = 0.223 \times 10^{-5} \text{ m}$

focal length change $\Delta f = 0.776 \times 10^{-5} \text{ m}$

rotation angle $\phi_x = 0.354 \times 10^{-10} \text{ rad}$ $\phi_y = -0.741 \times 10^{-10} \text{ rad}$

Case 2 horizon pointing 1

rms error =6.2 μm

vertex displacement $d_x = -0.493 \times 10^{-2} \text{ m}$ $d_y = 0.132 \times 10^{-9} \text{ m}$ $d_z = -0.263 \times 10^{-11} \text{ m}$

focal length change $\Delta f = 0.000 \times 10^{-8} \text{ m}$

rotation angle $\phi_x = 0.179 \times 10^{-10} \text{ rad}$ $\phi_y = 0.802 \times 10^{-3} \text{ rad}$

The surface and contour maps of the residual rms error of the calculated model are shown in Fig. 15 to 18. For this model the rms error when the antenna is pointed to zenith is 8 μm and when it is pointed to the horizon is 6 μm . The calculated variables of the fitted parabolas are in Table 6.

5.4 Static stress calculation under survival condition

For checking the structure stability, static analyses of the antenna structure under extreme survival conditions both when it is facing the wind and when the axis of the dish is perpendicular to the wind have been performed. The stress level of each member has been drawn in Fig. 17 and 18. It seems that stress of all members is far below the ultimate stress level of CFRP, which is $1.09 \times 10^9 \text{ N/m}^2$. However some member stress are high when the wind is from the side of the antenna. In these analyses, the loading has been simplified so the pressure on the panel surfaces is equal to the extreme pressure in both two cases. This makes the stress level when the wind is blowing on side of the dish higher than it should be. Further check and analysis of stress levels is still needed for the final design under different loading conditions and different orientations.

REFERENCES

- [1] National Radio Astronomy Observatory, The millimeter array-Proposal to the National Science Foundation, July 1990.
- [2] National Radio Astronomy Observatory, Millimeter array design and development plan, Sept 1992.
- [3] Hogg, D.E., A summary of data obtained during the mmA site survey, millimeter array memo No. 79, Feb, 1992.
- [4] Cheimets, P., Measurement of wind at Mauna Kea site, Tech. Memo. No 28 SMA project, Smithsonian Astronomy Center, 1990.
- [5] Lamb, J. and Payne J., Report on visit to HatCreek, MMA antenna memo 4, 1992.
- [6] Massion, C. et al, SMA design study, Harvard-Smithsonian Center for Astrophysics, 1992.
- [7] Ruze, J, Antenna tolerance theory a review, Proc. IEEE 54,633,1966
- [8] Cheng, J, Discussion of slant axis antennae concept, MMA memo 94, 1992.
- [9] Lamb, J, Effective surface error budget, 1992.
- [10] Hills, R., Analysis of designs of Tetrapod, JCMT memo, Nov. 1983.
- [11] Ogata, k., Modern control engineering, Prentice-Hall, Inc., Englewood Cliffs, N.J., 1970.
- [12] Lamb, J., Thermal considerations for mmA antenna, MMA memo, may 1992.
- [13] Delannoy, J., The design of high frequency antennas, IAU VCol. 131, Oct. 1990.
- [14] Findlay, J. W. and von Hoerner, S., A 65-meter telescope for millimeter wavelengths, NRAO, 1972.
- [15] Beards, C.F., Structural vibration analysis: modelling, analysis and damping of vibrating structures, Ellis Horwood Ltd., 1983.

APPENDIX

STIFFNESS OF SERRURIER-TYPE TRUSS STRUCTURE

The Surrurier truss structure was developed specially for the top end support of an optical telescope tube. A standard Serrurier truss has four sides and eight beam members as shown in Fig. A1. Serrurier truss structure has been used for almost all optical telescope tube designs since it has a high rigidity in all directions and results a parallel displacement pattern of the secondary mirror. The Serrurier-type truss has been used for the JCMT secondary mirror support. In the MMA antenna design, Surrurier-type trusses are also used both for its secondary mirror support and the backup structure center ring support(see Fig. A2). However, the trusses used in the MMA antenna have their side number different from four. In order to design a rigid and efficient structure, it is important to determine which kind of Serrurier-type design is more rigid and more cost effective. In this appendix, the torsional stiffness of the Serrurier-type trusses with different numbers of sides is discussed in detail. Torsional stiffness is in most cases a more important parameter in the truss design, since in other directions, rigidity of trusses are easy to calculate.

Assume the supporting truss has its base radius as $R_2 = R$ (ref. Fig. A3), the supported ring radius as $R_1 = \epsilon R$, and the height of the structure as $H = \xi R$. If the truss structure has n sides, then there will be $2n$ beam members. Let L represent the member length of the truss. The structure torsional natural frequency can be represented by the following formula:

$$\omega = (K / J)^{1/2}$$

where K is structural stiffness and J is the moment of inertia of the mass it supports. The torsional stiffness of the structure is:

$$K=2nEA(L_1^2R_1^2/L^2)$$

where E is Young's modules, A is member cross-section area. L_1 is defined in Fig. A3.

Since the weight of the structure could be represented as:

$$W=2nLA$$

so $K = (L_1^2R_1^2/L^3)WE$

where $L_1=R_2 \sin(\pi/n)$ and $L = (H_2^2+R_1^2+R_2^2-2R_1R_2 \cos(\pi/n))^{1/2}$

By choosing different ϵ and ξ , relative structure stiffness can be calculated by assuming W and E are constant for all the cases. The calculation results are shown in Figs. A4-A10. Fig. A4 is the relative stiffness of trusses with different side number for the case when ξ is equal to zero. Fig. A5 is the relative stiffness of trusses when ξ is equal to 0.5 and Fig.A6 is the relative stiffness of trusses when ξ is equal to 1. Fig A7 is the the relative stiffness of trusses when the truss side number is three sides. And Figs. 8-10 are those when the truss

side numbers are four, five and six respectively. In Figures 7-10, alpha0 line is for the case where $\xi=0$, alpha05 line is for the case where $\xi=0.5$ and alpha10 line is for the case where $\xi=1.0$.

From these figures, the conclusions are:

a) For all cases, the torsional stiffness of the structure firstly increases from zero as the R_1 , R_2 ratio increases, they reach their maximum when the ratio is near unity. Afterwards, the stiffness will decrease as the R ratio increases.

b) If the R ratio is near unity, then the stiffness of the structure will increase as the side number increases if the structure height is not so big ($\xi < 0.5$).

c) For higher structure ($\xi=1$), three side structure is stiffer than those with larger side numbers.

d) If radius ratio is small ($R_1/R_2 < 0.4$), three side structure is always more effective than trusses with more sides and members.

f) Larger radius ratio ($R_1/R_2 > 2$) and larger side number always results a lower structure stiffness. Three side structure results a more flat stiffness curve and can be used for wide range radius ratio.

g) Calculation also shows that very large radius ratio always causes lower stiffness of the structure.

FIGURE CAPTIONS

- Figure 1 Perspective view of proposed MMA antenna structure
- Figure 2 Perspective view of MMA antenna when it is pointing horizon
- Figure 3 MMA antenna panel arrangement and their support nodes
- Figure 4 Two simple models of secondary mirror supports used for NASTRAN analysis
- Figure 5 MMA antenna dish structure NASTRAN model for analysis
- Figure 6 MMA dish structure vibration mode 1
- Figure 7 MMA dish structure vibration mode 2
- Figure 8 MMA dish structure vibration mode 3
- Figure 9 MMA antenna NASTRAN model for analysis
- Figure 10 MMA antenna vibration mode 1
- Figure 11 BIMA 6-m Cassegrain antenna structure
- Figure 12 SMA 6-m bent-Nasmyth antenna structure
- Figure 13 First six mode of vibration of an elevation axis support structure(Fig. 26 of 65-m telescope report of Findlay and von Hoerner)
- Figure 14 The front part of the backup structure, the squares are joint nodes mass element
- Figure 15 The middle part of the backup structure
- Figure 14 The back and bottom parts of the backup structure, the squares are joint nodes mass element
- Figure 15 The residual fitting results of the backup structure model when it is at zenith pointing
- Figure 16 The residual fitting results of the backup structure model when it is at horizon pointing(surface pattern)
- Figure 17 The residual fitting results of the backup structure model when it is at horizon pointing(contour map)
- Figure 18 The residual fitting results of the backup structure model when it is at zenith pointing(surface pattern)
- Figure 19 The stress of each member when the antenna under extreme loading is facing the dish(contour map)
- Figure 20 The stress of each member when the antenna under extreme loading is from side of the dish
- Figure A1 Serrurier truss structure used in optical telescope tube
- Figure A2 Serrurier-type trusses used at MMA antenna backup structure
- Figure A3 Truss parameters definition
- Figure A4 Stiffness of truss structures with different side number when ξ is zero
- Figure A5 Stiffness of truss structures with different side number when ξ is 0.5
- Figure A6 Stiffness of truss structures with different side number when ξ is 1.0

Figure A7 Stiffness of three side six beam truss structures with different ξ number

Figure A8 Stiffness of four side eight beam truss structures with different * number

Figure A9 Stiffness of five side ten beam truss structures with different * number

Figure A10 Stiffness of six side twelve beam truss structures with different * number

TABLE CAPTIONS

Table 1 Breakdown of antenna structural weight

Table 2 Panel geometry and related data

Table 3 Stiffness of 2-m Rotex grade G0 cross-roller bearing

Table 4 The results of antenna dynamic analysis

Table 5 Weight estimation of different design concepts

Table 6 The best fit result of an backup structure model

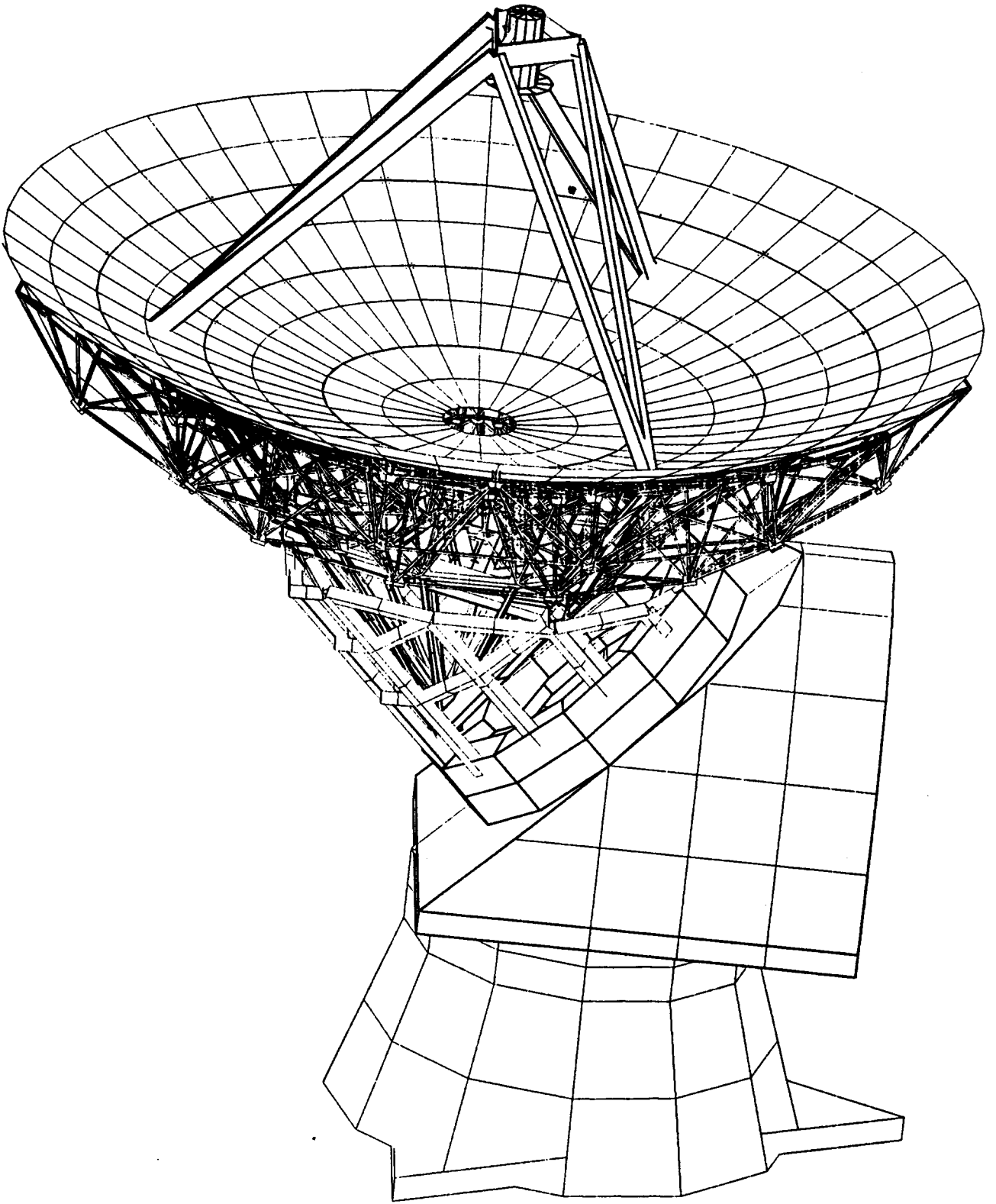


Figure 1 Perspective view of proposed MMA antenna structure

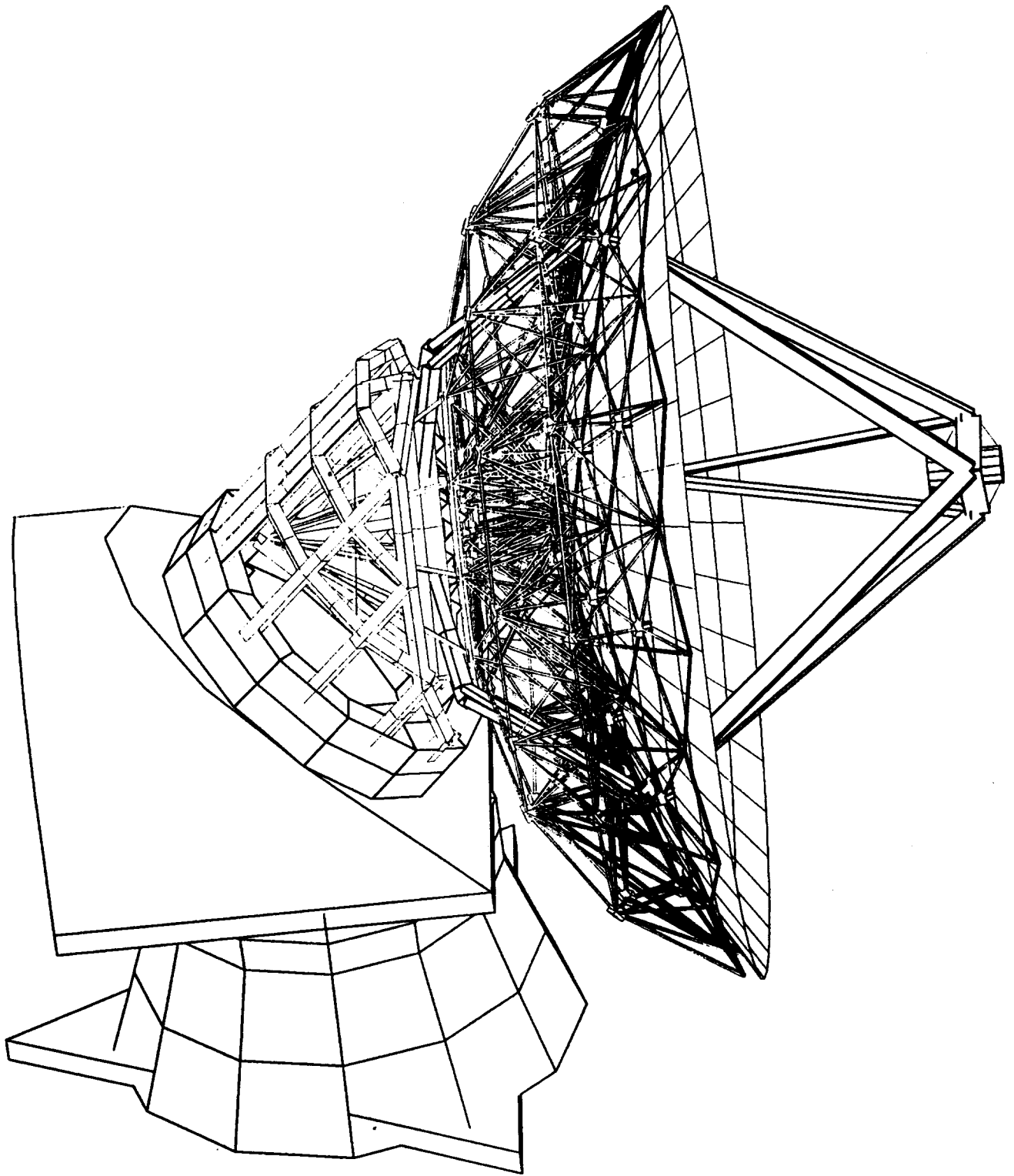


Figure 2 Perspective view of MMA antenna when it is pointing horizon

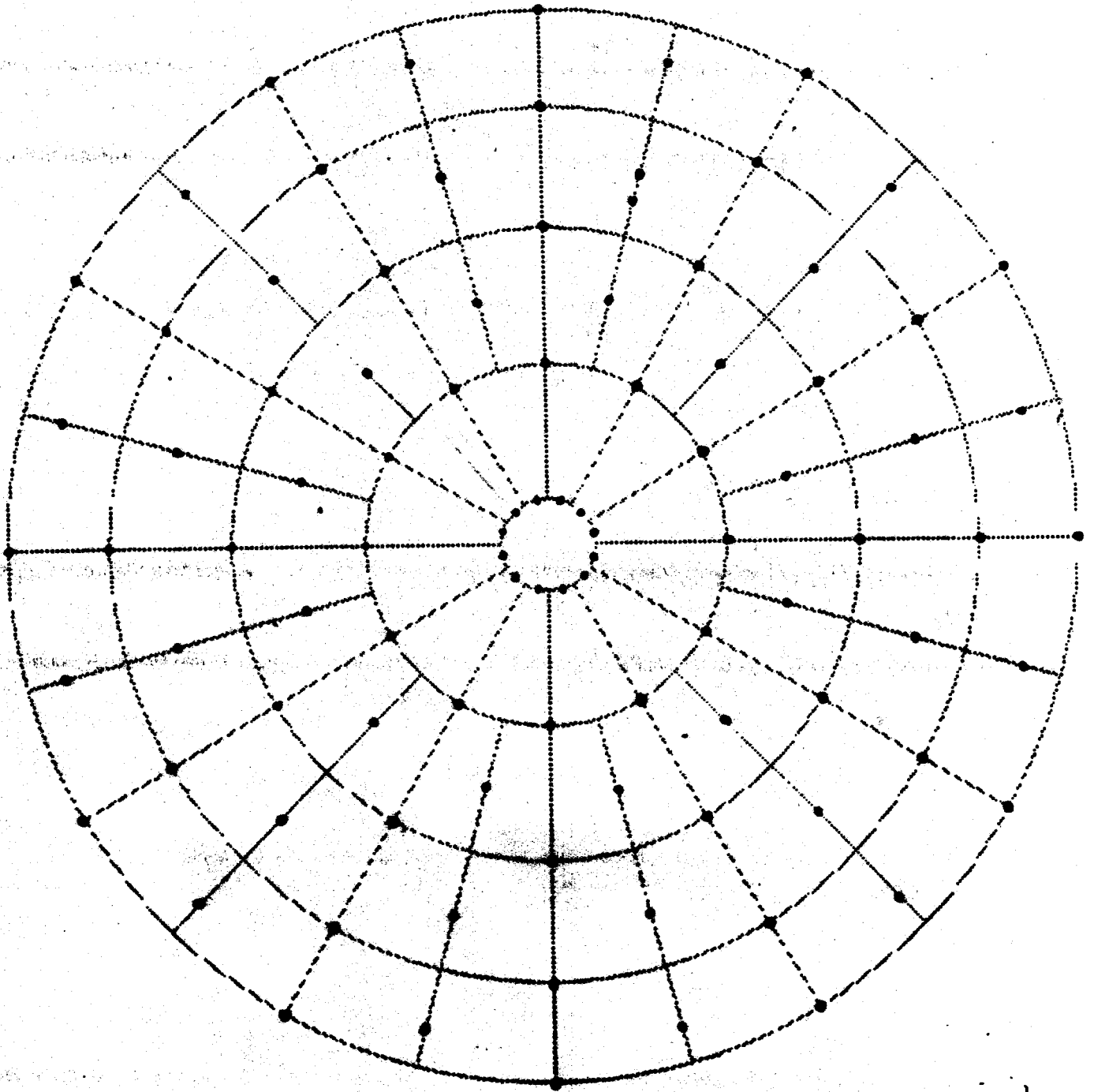


Figure 3 MMA antenna panel arrangement and their support nodes

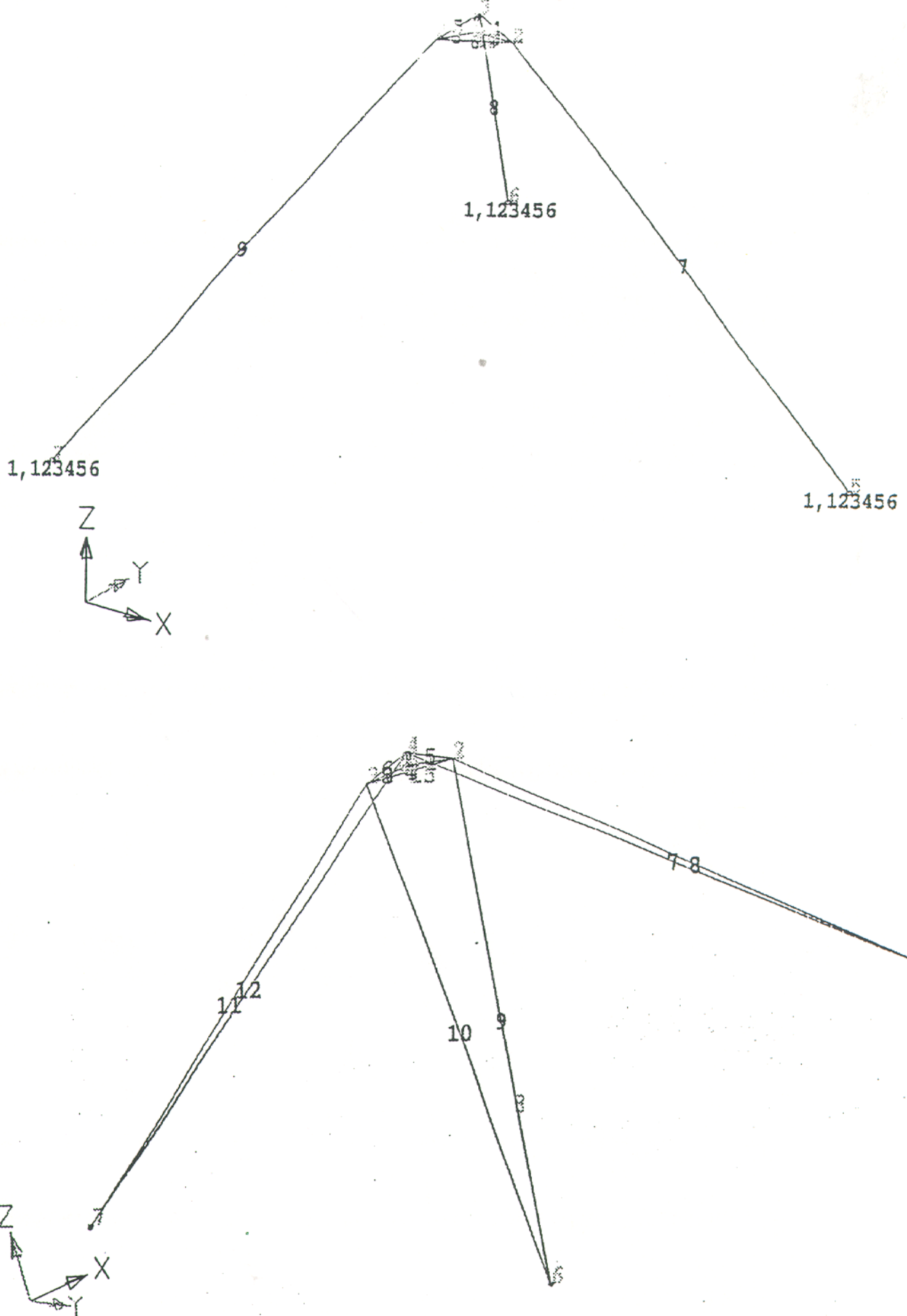


Figure 4 Two simple models of secondary mirror supports used for NASTRAN analysis

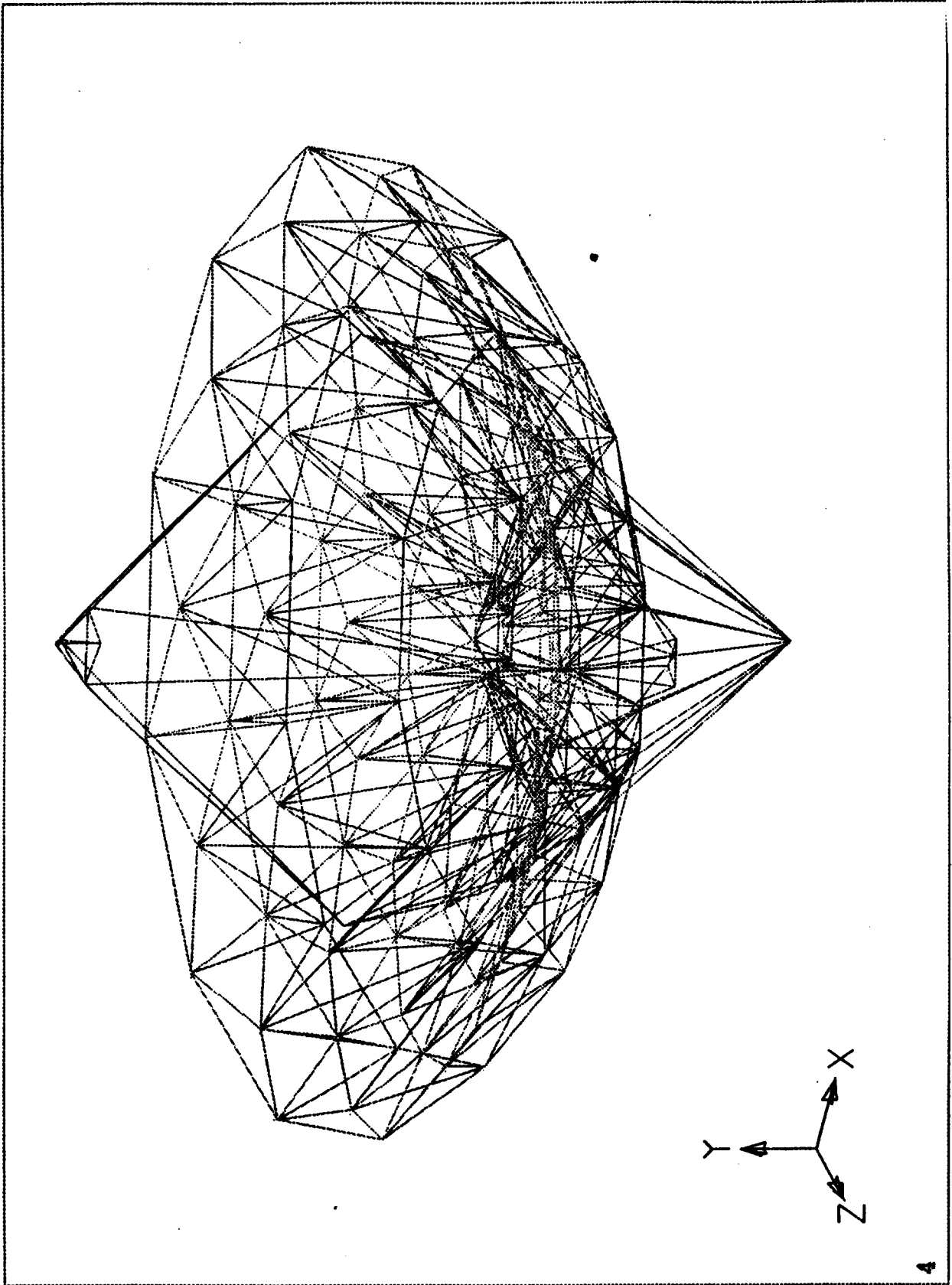


Figure 5 MMA antenna dish structure NASTRAN model for analysis

MSC/XL V3A

16 Apr 92

Database:part12d.xdb

Application:MSC/NASTRAN

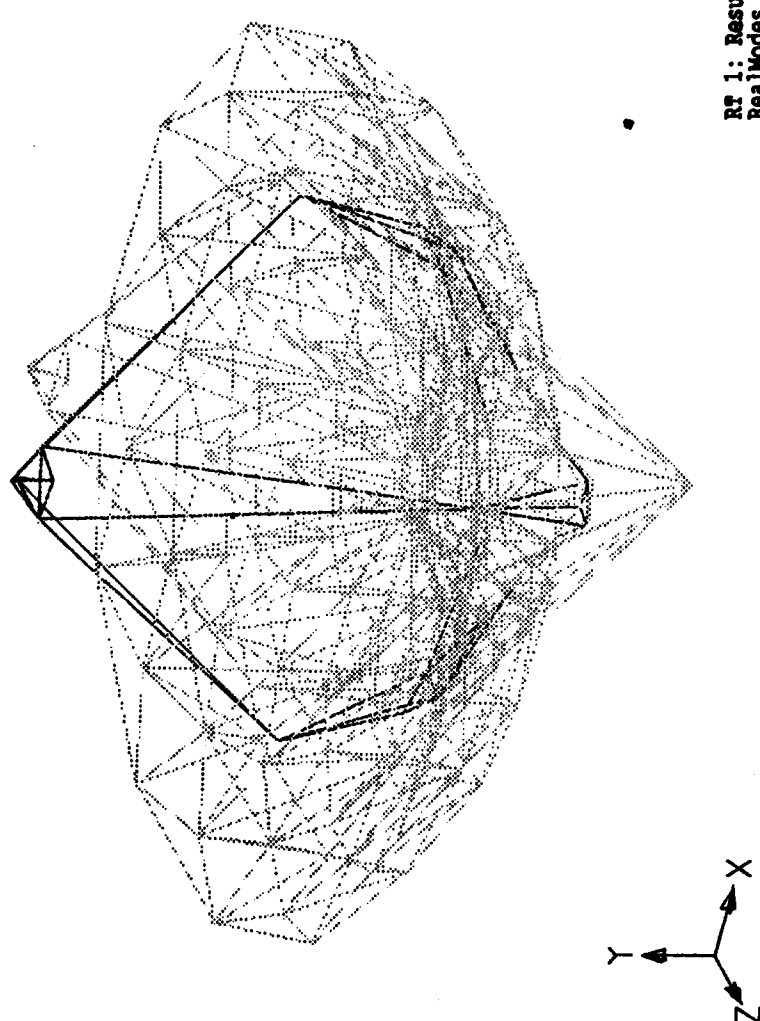
| | |
|---|--|
| <p>View 4 Part 0 Tables Tools Geometry FEM Analysis XF Plotting Interface with</p> | <p>Ref/Wireframe Create Qual Undo Help Exit</p> |
| <p>ResultsTable 1 ColorRange 1 Title .1 Contours Animate Graph 1 Arrow Export</p> |  |
| <p>AutoScale On Scale By 13.6139 QuickEditRT Def. Color Yellow Undef. Color Red Deformed On Plot In View 4 Erase View 4</p> | <p>RT 1: ResultsDB RealModes Analysis Subcase 1 Mode 1 Def. Subcase 1</p> <p>Done-> Replay On /Erase Done-> Edit DisplayTable/1 BoundaryColoringMode=GlobalColor /Modify/NoReset Done-> Edit ColorTable/1 Global=Yellow /Modify/NoReset Done-> Refresh View/4 /NoFind/NoErase/NoCenter/Complete/Wireframe/Deformed/NoPlot Done-> Edit DisplayTable/1 BoundaryColoringMode=Elementtype /Modify/NoReset Done-> Edit ColorTable/1 Global=White /Modify/NoReset replay off</p> |

Figure 6 MMA dish structure vibration mode 1

MSC/XL V3A
16 Apr 92

Database: part12d.xdb
Application: MSC/NASTRAN

| | | | |
|--|---|---|---|
| <p>View 4 Part 0 Tables Tools Geometry FEM Analysis XY Plotting Interface with</p> | <p>ResultTable 1 ColorRange 1 Title 1 Contours Animate Graph 1 Arrow Export</p> | <p>AutoScale On Scale By 13.6139 QuickEditRT Def. Color Yellow Undef. Color Red Deformed On Plot In View 4 Grase View 4</p> | <p>4 Done-> Replay On /Grase Done-> Edit DisplayTable/1 BoundaryColoringMode=GlobalColor /Modify/NoReset Done-> Edit ColorTable/1 Global=Yellow /Modify/NoReset Done-> Refresh View/4 /NoFind/NoErase/NoCenter/Complete/Wireframe/Deformed/NoPlo Done-> Edit DisplayTable/1 BoundaryColoringMode=Elementtype /Modify/NoReset Done-> Edit ColorTable/1 Global=White /Modify/NoReset replay off</p> |
| | | <p>RF 1: ResultsDB RealModes Analysis Subcase 1 Mode 2 Def. Subcase 1</p> | |
| <p>Ref/Wireframe Create Qual Undo Help</p> | | <p>Exit</p> | |

Figure 7 MMA dish structure vibration mode 2

MSC/XL V3A
16 Apr 92

Database: part12d.xdb
Application: MSC/NASTRAN

| | | | | | | | | | | | | | |
|---|--|--|--|---|--|--|--|---|--|--|--|---|--|
| View 4 | | Ref/Wireframe | | Create Qual | | Undo | | Help | | Exit | | | |
| <ul style="list-style-type: none"> Part 0 Tables Tools Geometry FEM Analysis XY Plotting Interface with | | <ul style="list-style-type: none"> ResultsTable 1 ColorRange 1 Title 1 Contours Deform Animate Graph 1 Arrow Export | | <ul style="list-style-type: none"> Grid Displa ElitD Grid Elit2D Grid Plot In View 4 Subcase 1 ModeNumber 3 | | <ul style="list-style-type: none"> 2 3 4 5 6 7 | | <ul style="list-style-type: none"> tTrans s s s s s | | <p>AutoScale On Scale By 24.7006 QuickEditRT</p> | | <p>RT 1: ResultsDB RealModes Analysis Subcase 1 Mode 3 Def. Subcase 1</p> | |
| | | | | | | | | | | | | | |
| <p>Done-> Edit ResultsTable/1 SuperElementList=0 ModeNumber=3 /Modify Done-> Edit DisplayTable/1 BoundaryColoringMode=GlobalColor /Modify/NoReset Done-> Edit ColorTable/1 Global=yellow /Modify/NoReset Done-> Refresh View/4 /NoFind/NoRaise/NoCenter/Complete/WireFrame/Deformed/NoPlot Done-> Edit DisplayTable/1 BoundaryColoringMode=Elementtype /Modify/NoReset Done-> Edit ColorTable/1 Global=White /Modify/NoReset >replay off</p> | | | | | | | | | | | | | |

Figure 8 MMA dish structure vibration mode 3

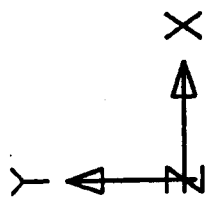
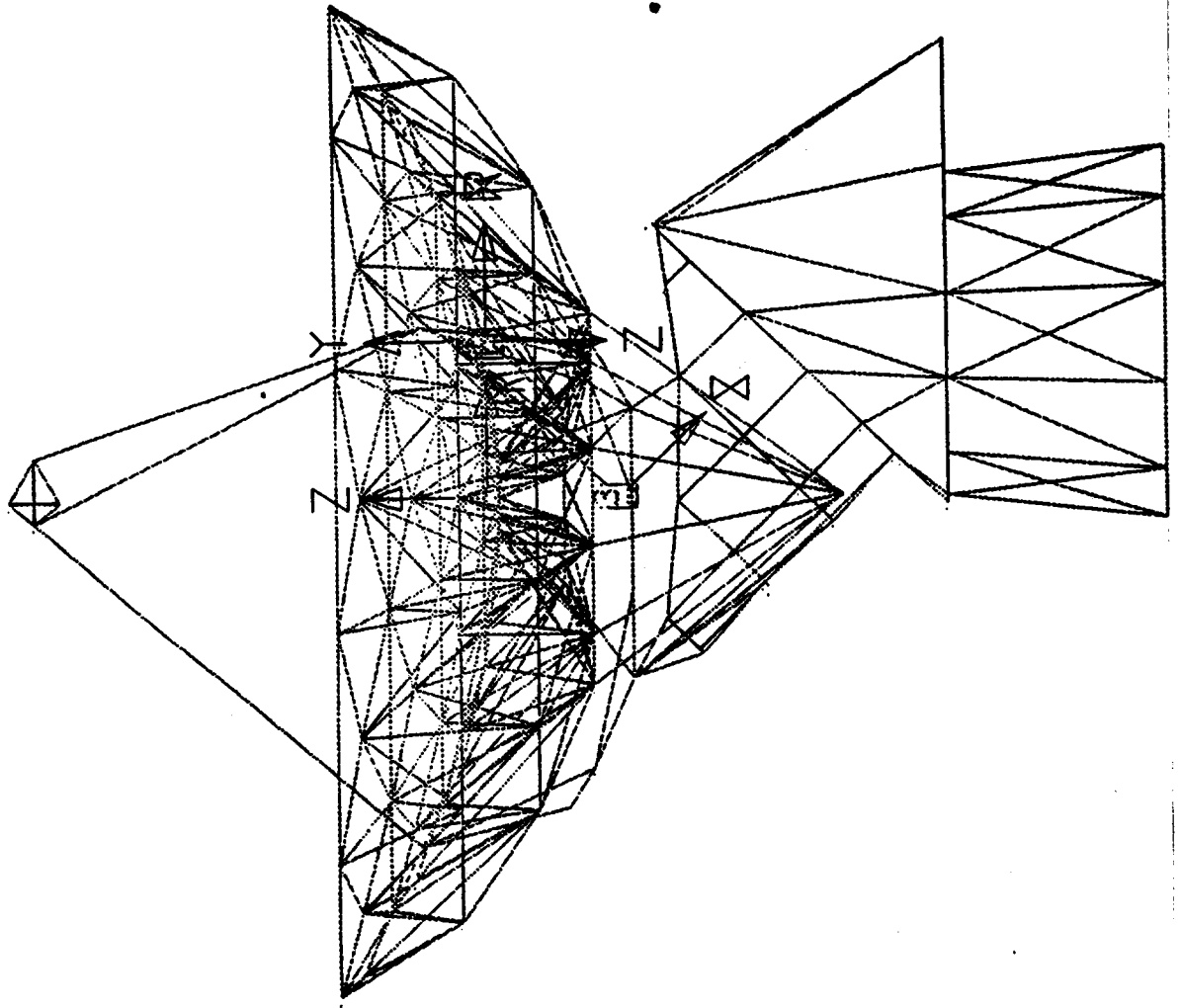


Figure 9 MMA antenna NASTRAN model for analysis

MSC/XL V3A
16 Apr 92

Database: v01d.xdb
Application: MSC/NASTRAN

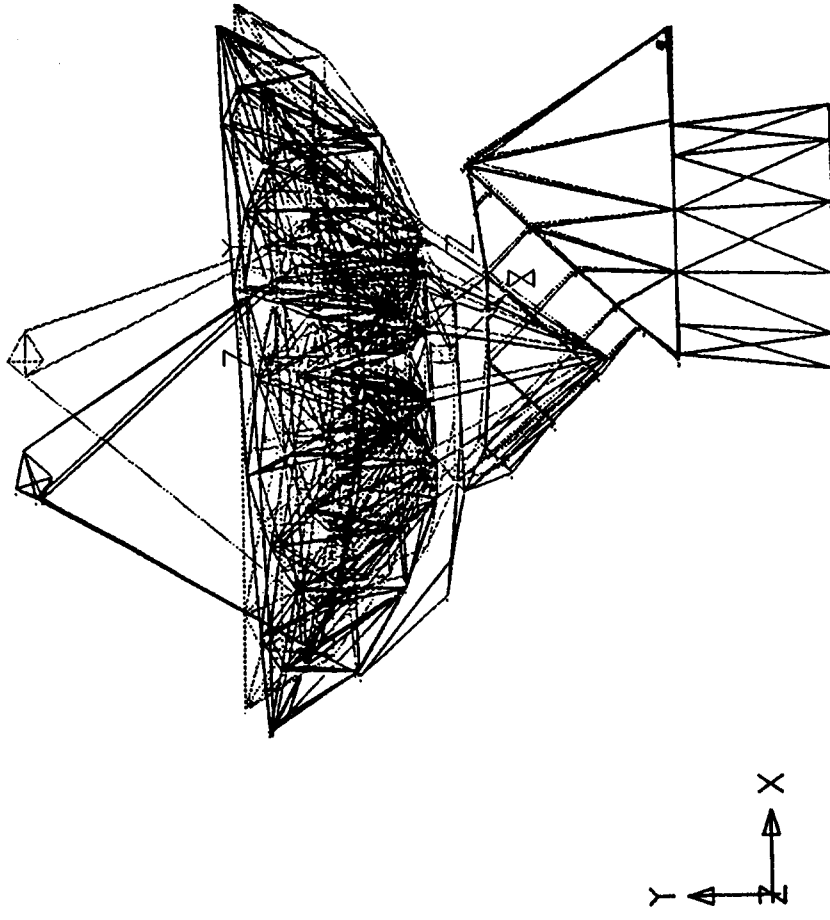
| | | | |
|---|--|--|--|
| <p>View 1 Part 0 Tables Tools Geometry FEM Analysis XY Plotting Interface with</p> | | <p>Ref/WireFrame Create Qual Undo Help Exit</p> | |
| <p>ResultsTable 1 ColorRange 1 Title 1 Contours Deformed Animate Graph 1 Arrow Export</p> | |  | |
| <p>AutoScale On Scale By 23.6167 QuickEditRT Def. Color White Undef. Color Blue Deformed On</p> | | <p>RT 1: ResultsDB RealModes Analysis Subcase 1 Mode 1 Def. Subcase 1</p> | |
| <p>Plot In View 1 Erase View 1</p> | | <p>Done-> Edit DisplayTable/1 BoundaryColoringMode=ElementType /Modify/NoReset replay on Done-> Replay On /Erase Done-> Edit DisplayTable/1 BoundaryColoringMode=GlobalColor /Modify/NoReset Done-> Refresh View/1 /NoFind/NoErase/NoCenter/Complete/FireFrame/Deformed/NoPlot Done-> Edit DisplayTable/1 BoundaryColoringMode=ElementType /Modify/NoReset replay off</p> | |

Figure 10 MMA antenna vibration mode 1

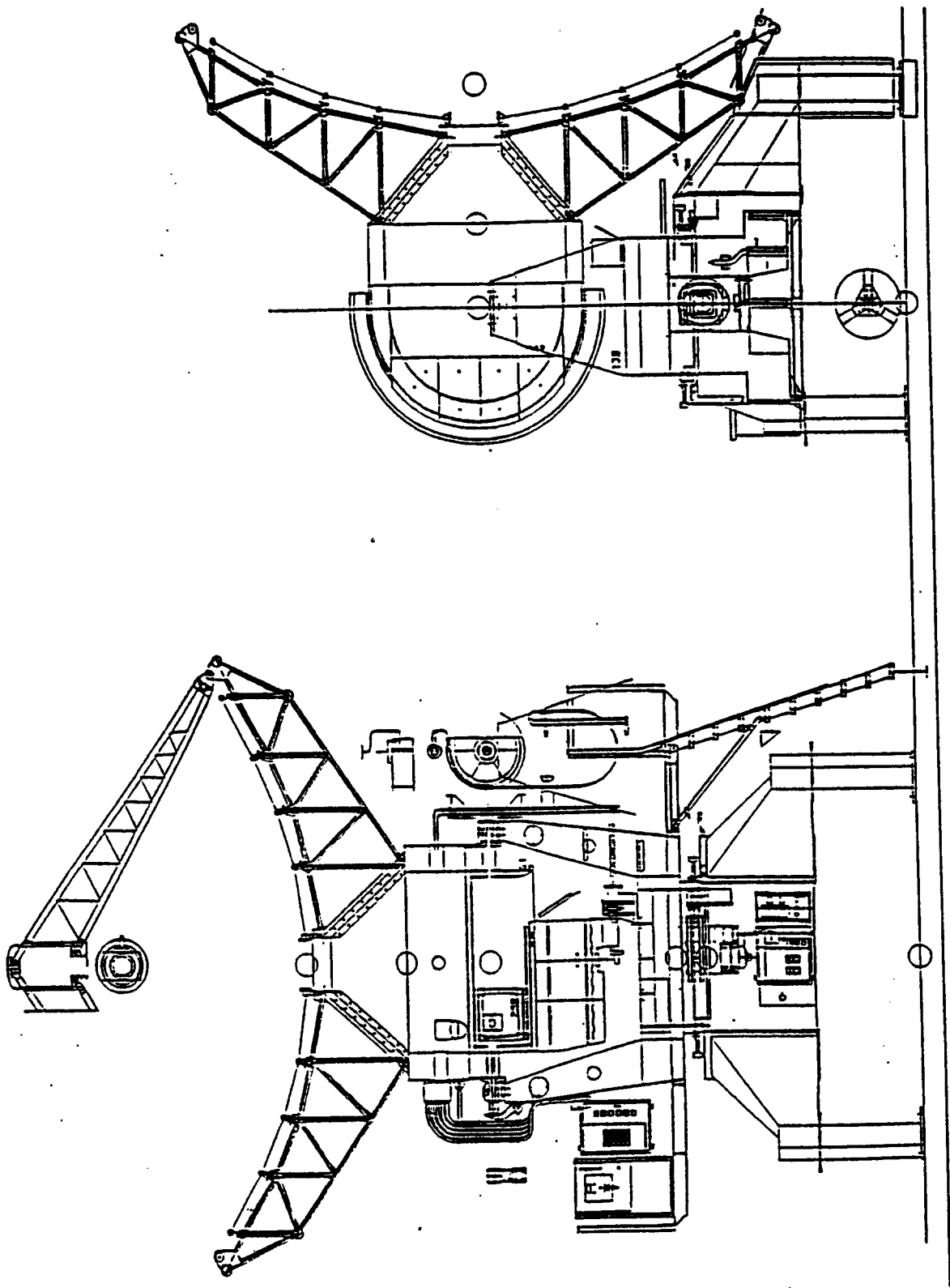


Figure 11 BIMA 6-m Cassegrain antenna structure

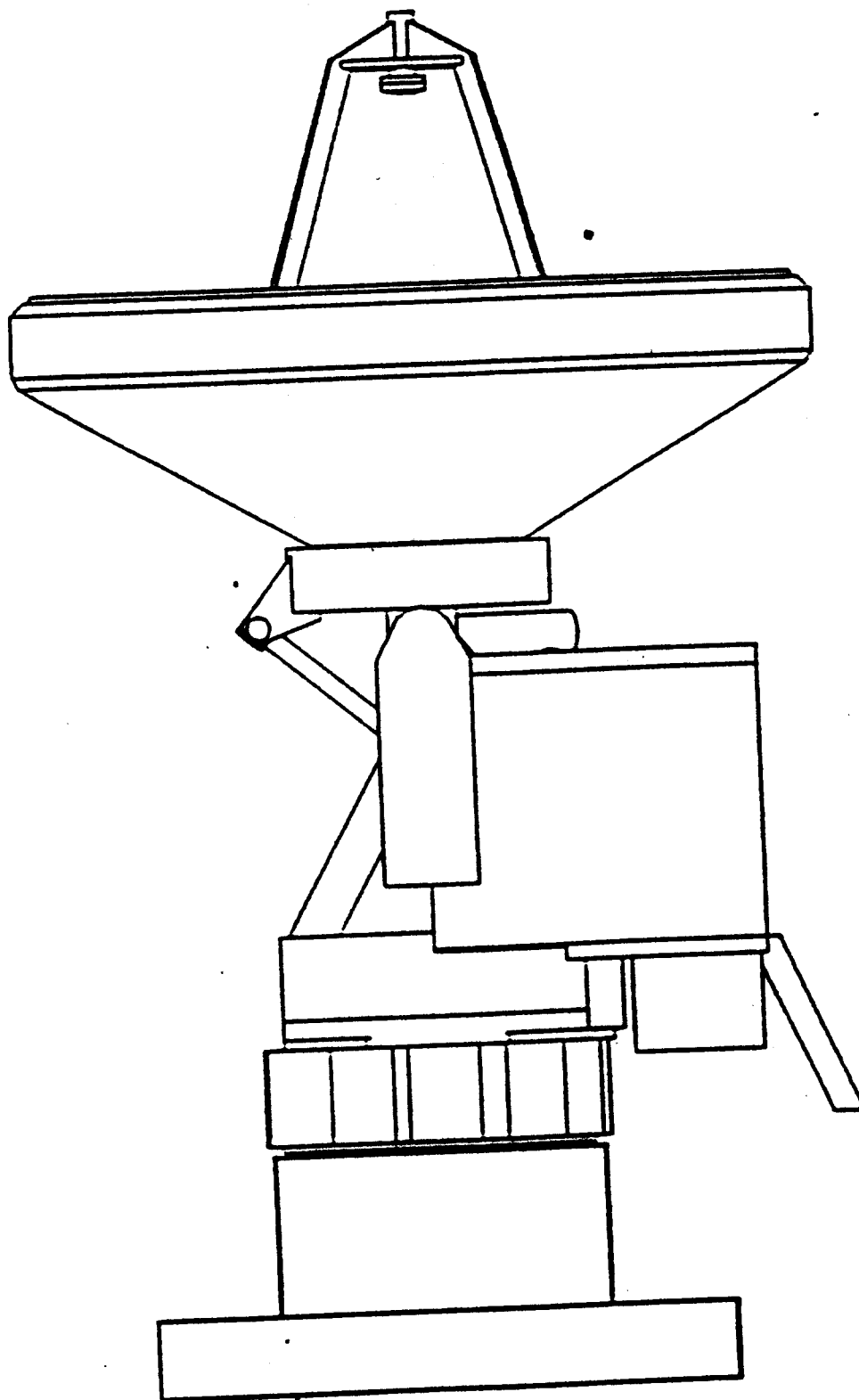


Figure 12 SMA 6-m bent-Nasmyth antenna structure

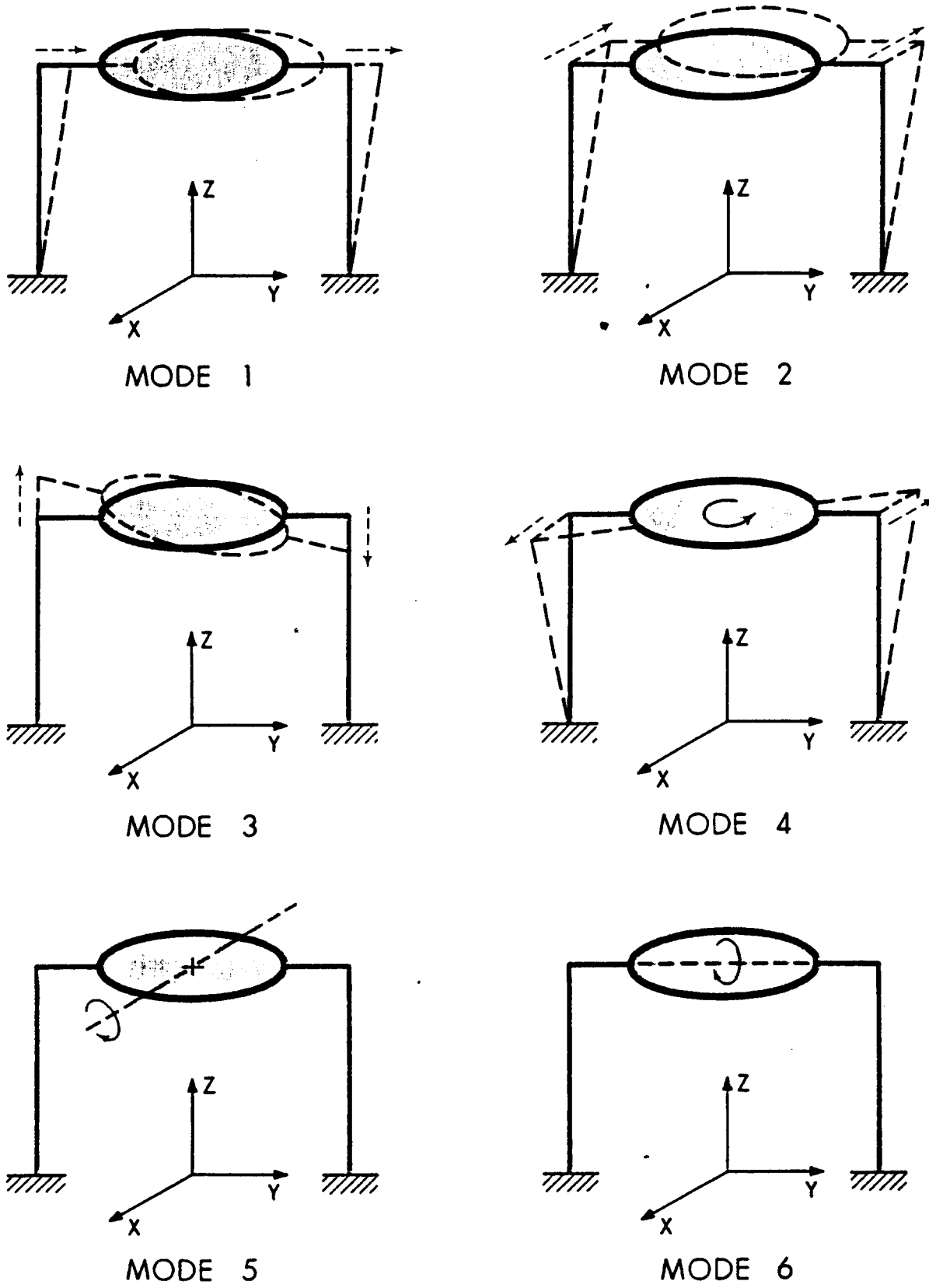


Figure 13 First six mode of vibration of an elevation axis support structure(Fig. 26 of 65-m telescope report of Findlay and von Hoerner)

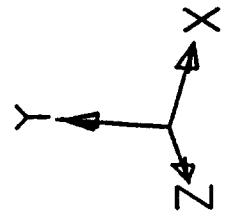
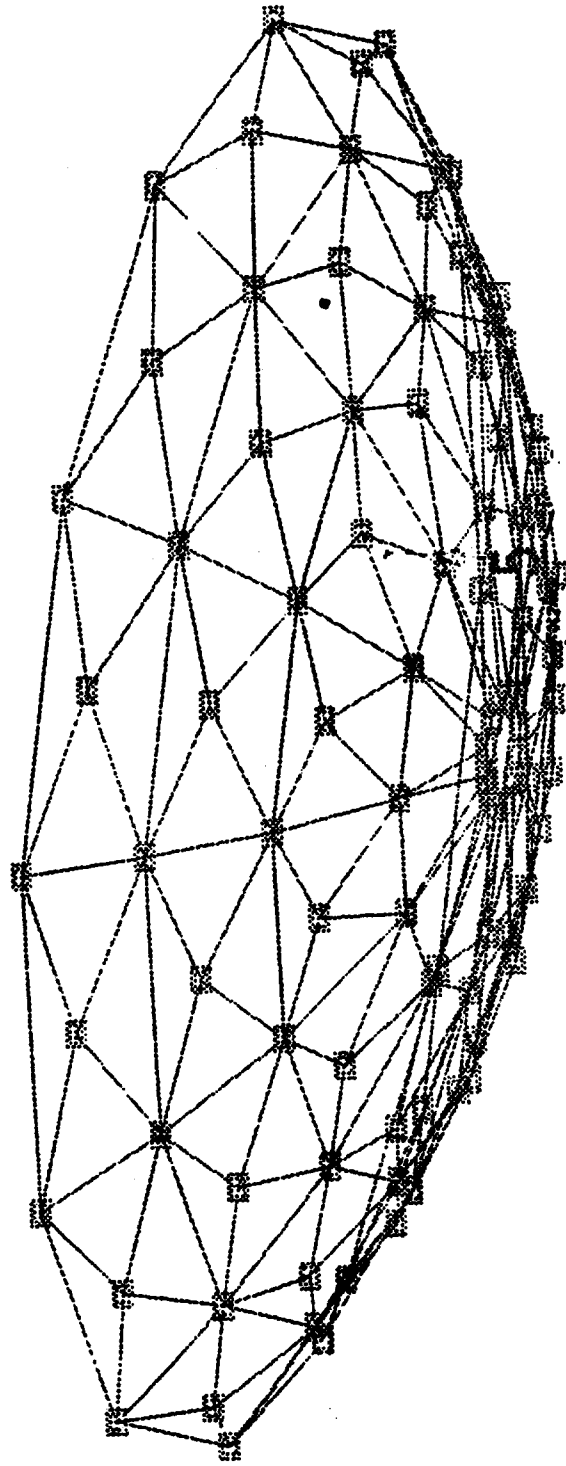


Figure 14 The front part of the backup structure, the squares are joint nodes mass element

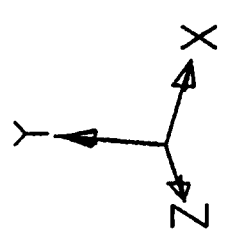
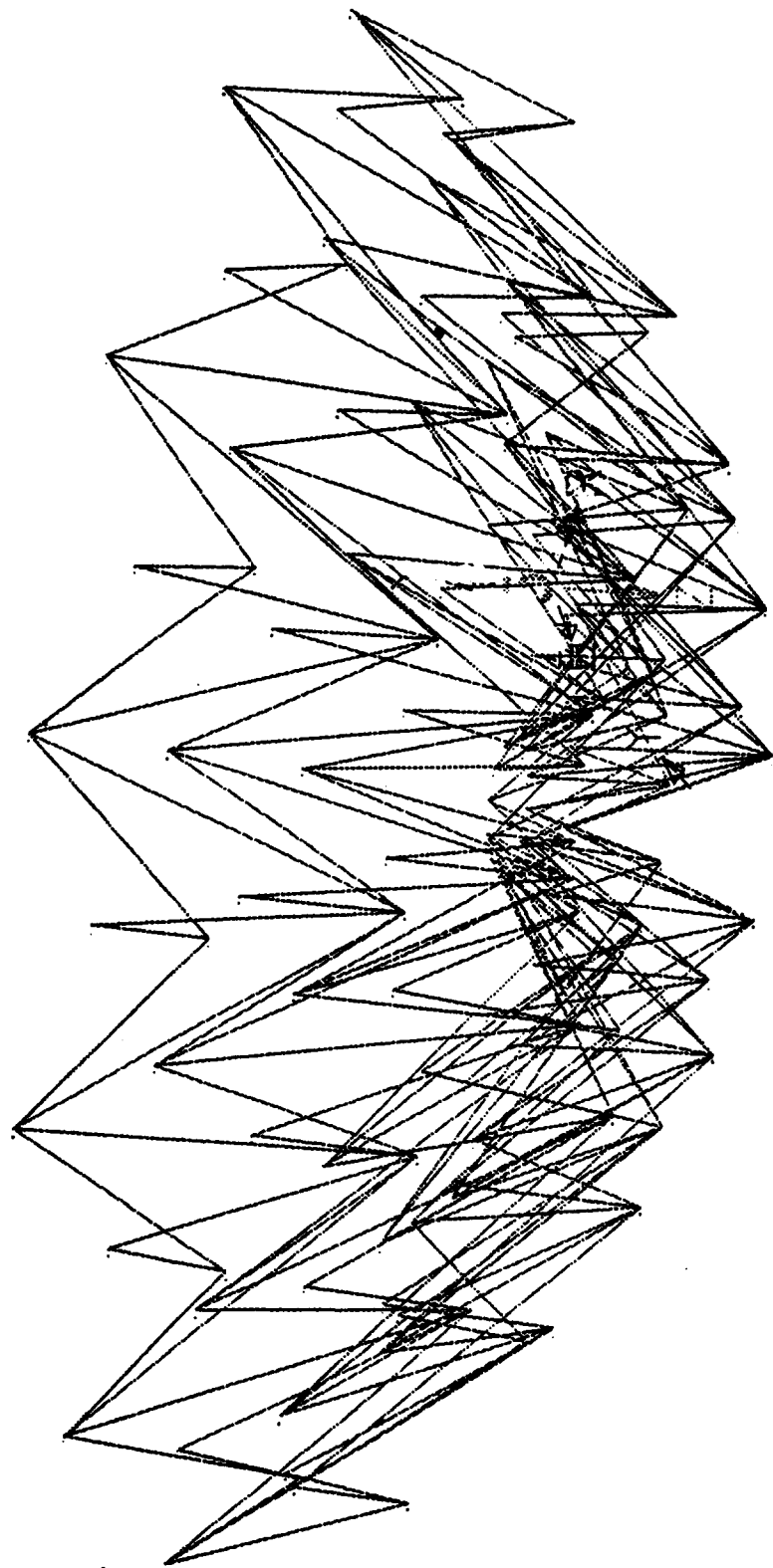


Figure 15 The middle part of the backup structure

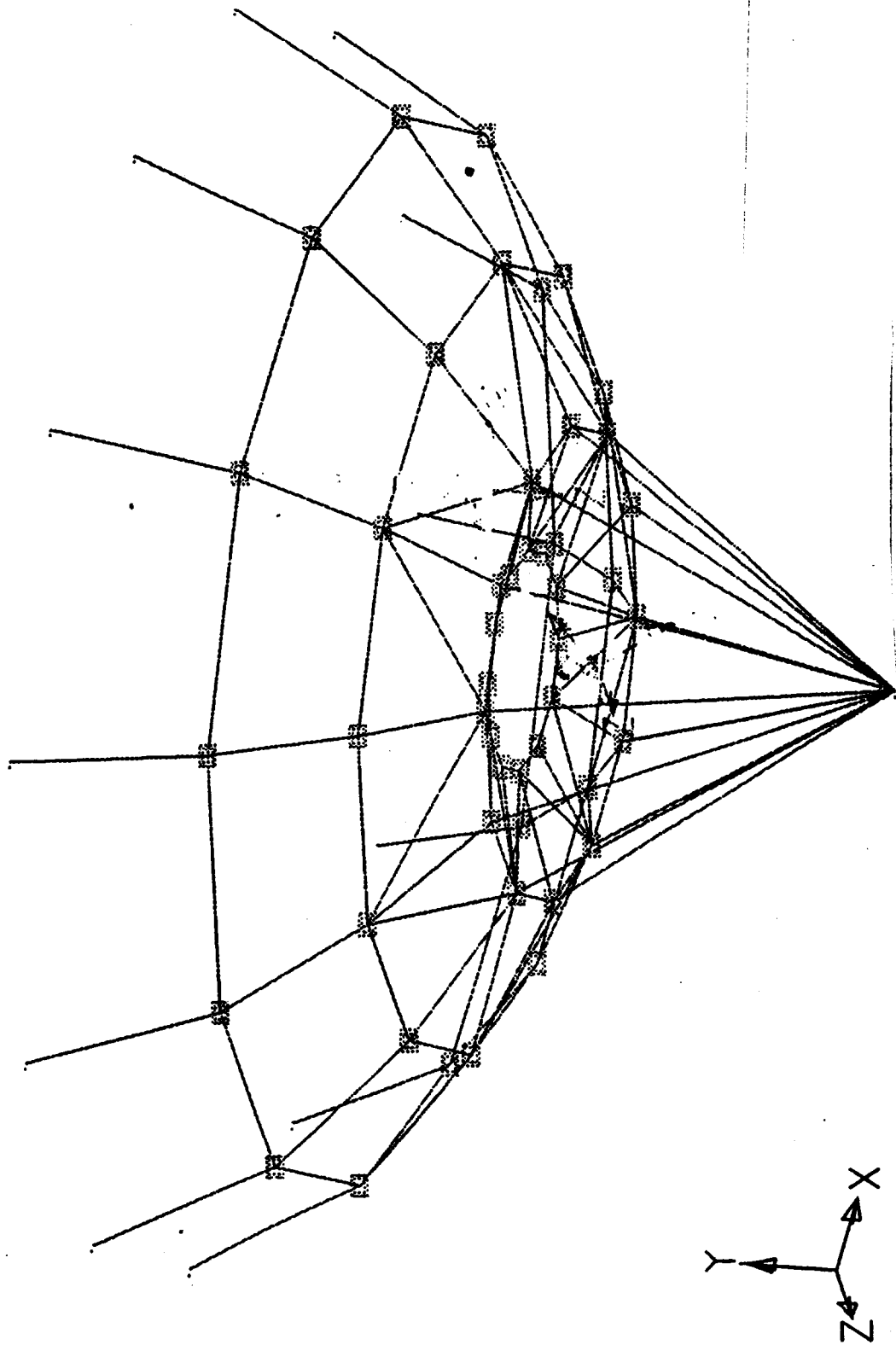


Figure 14 The back and bottom parts of the backup structure, the squares are joint nodes mass element

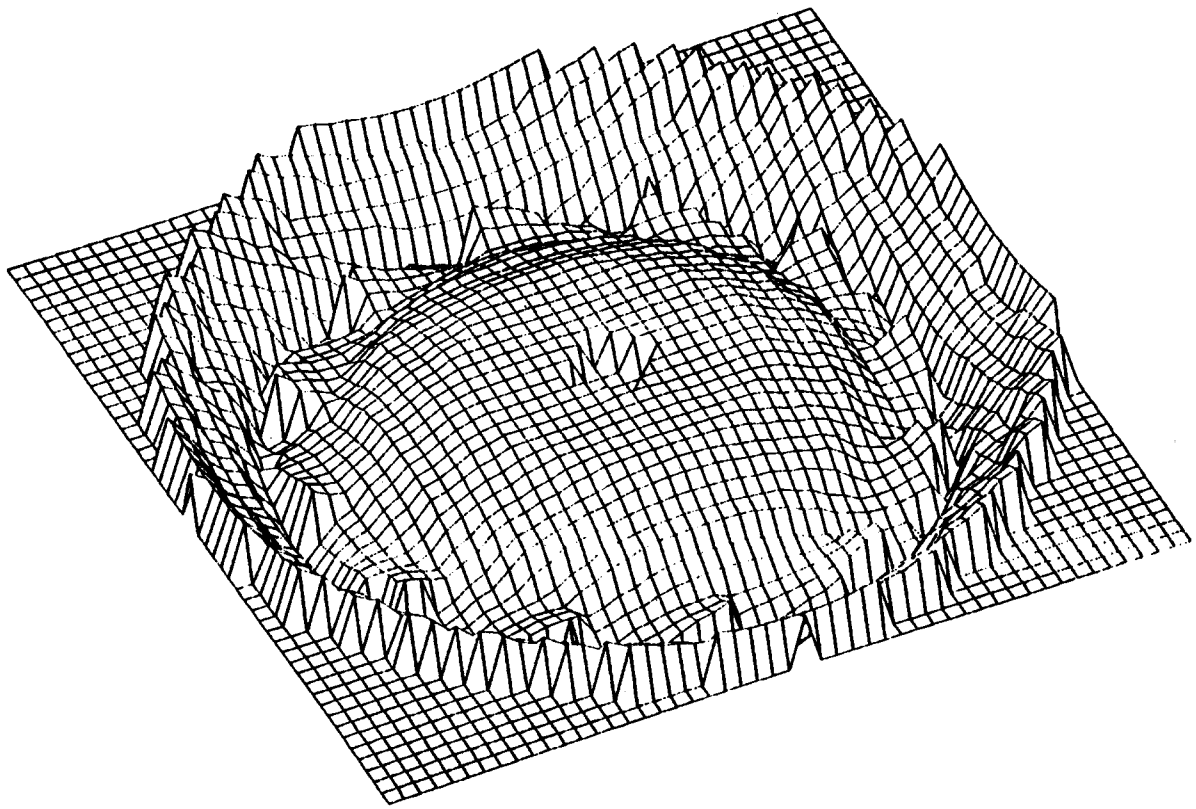


Figure 15 The residual fitting results of the backup structure model when it is at zenith pointing(surface pattern)

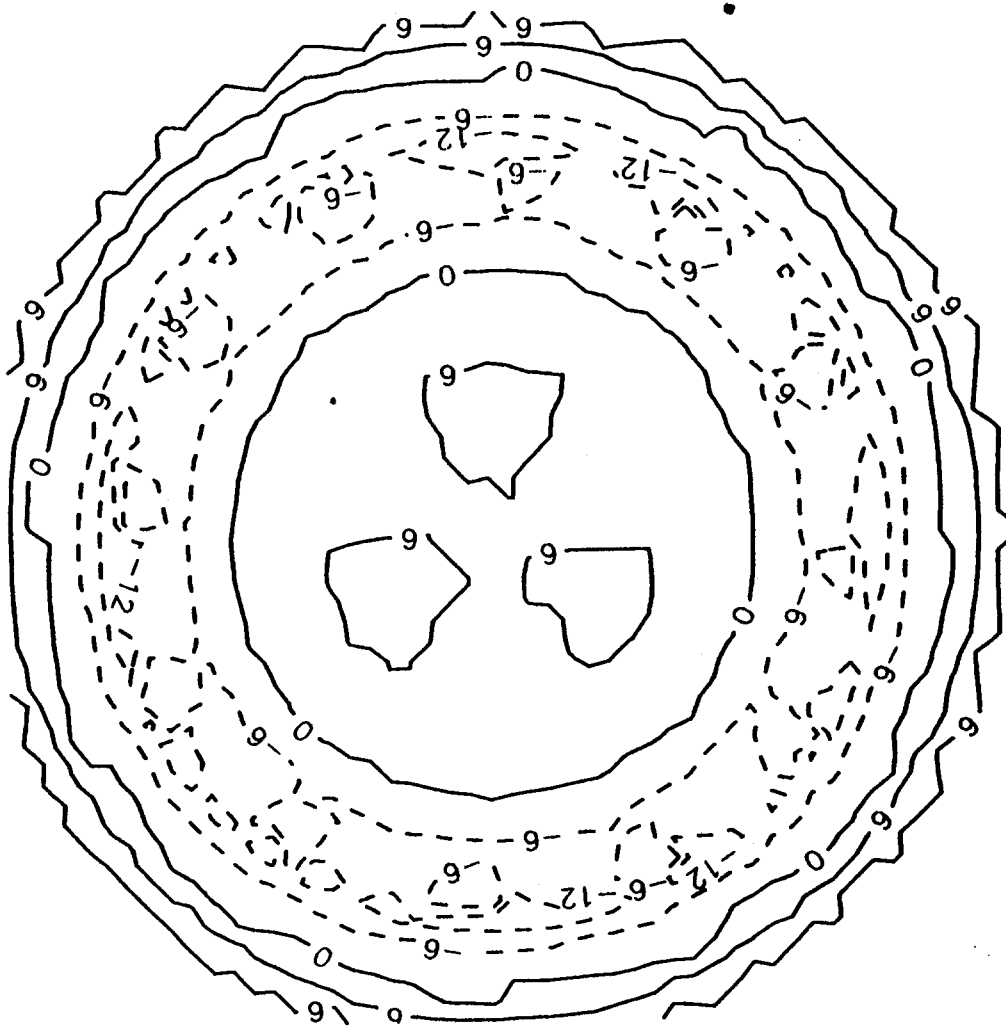


Figure 16 The residual fitting results of the backup structure model when it is at zenith pointing(contour map)

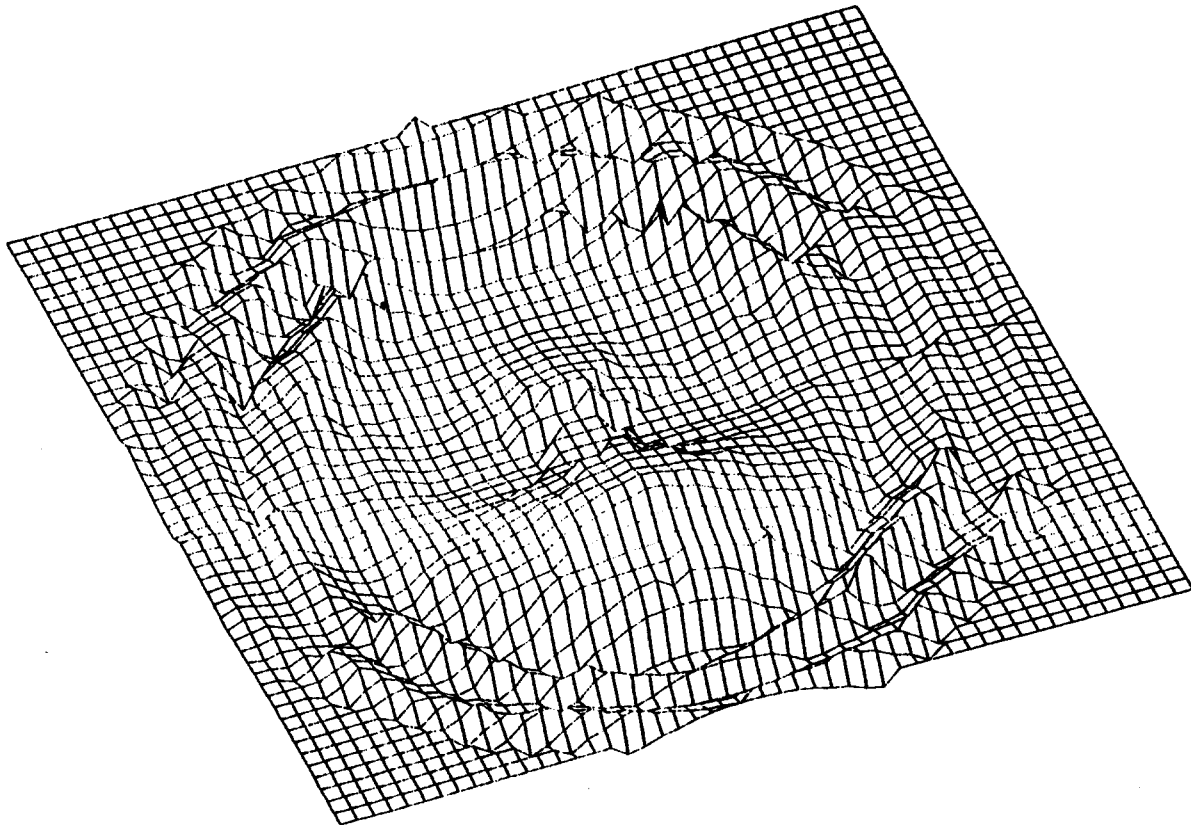


Figure 17 The residual fitting results of the backup structure model when it is at horizon pointing(surface pattern)

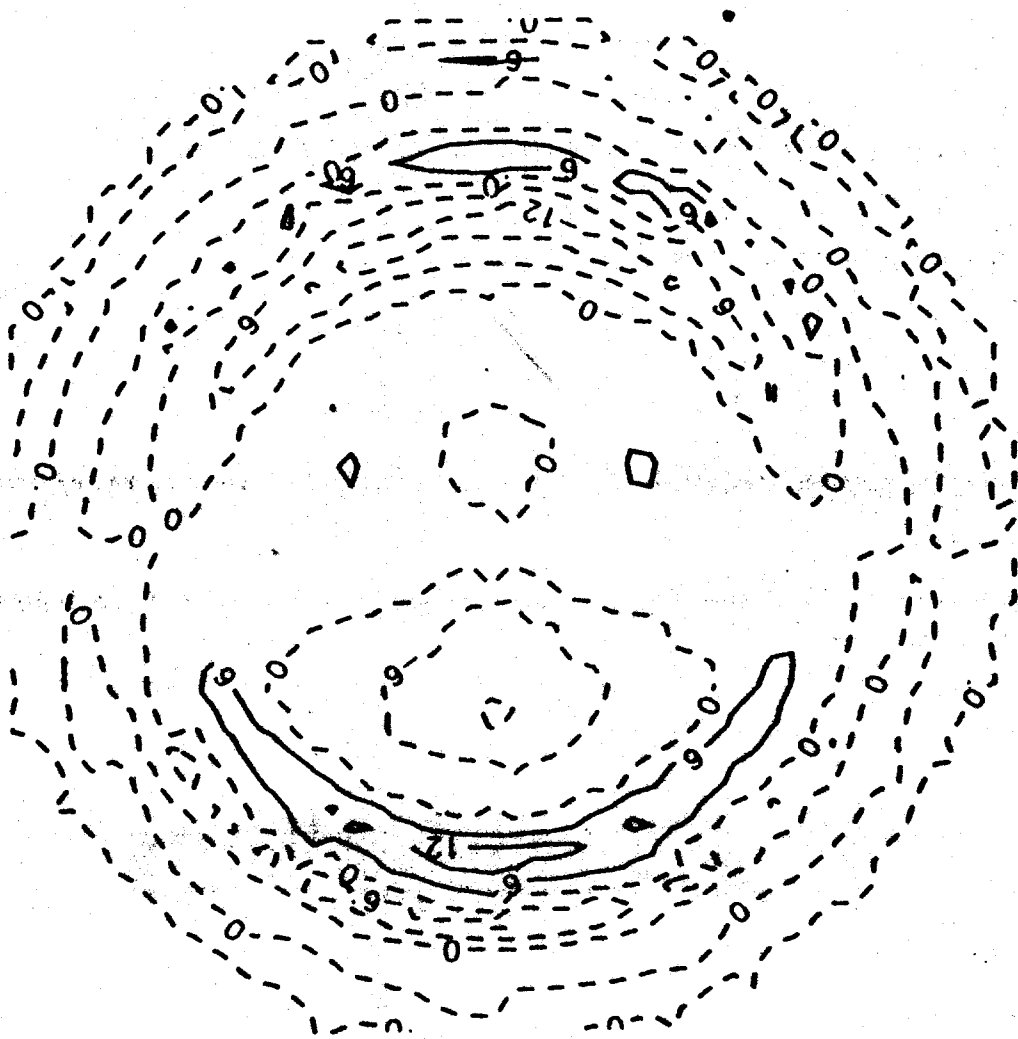


Figure 18 The residual fitting results of the backup structure model when it is at horizon pointing(contour map)

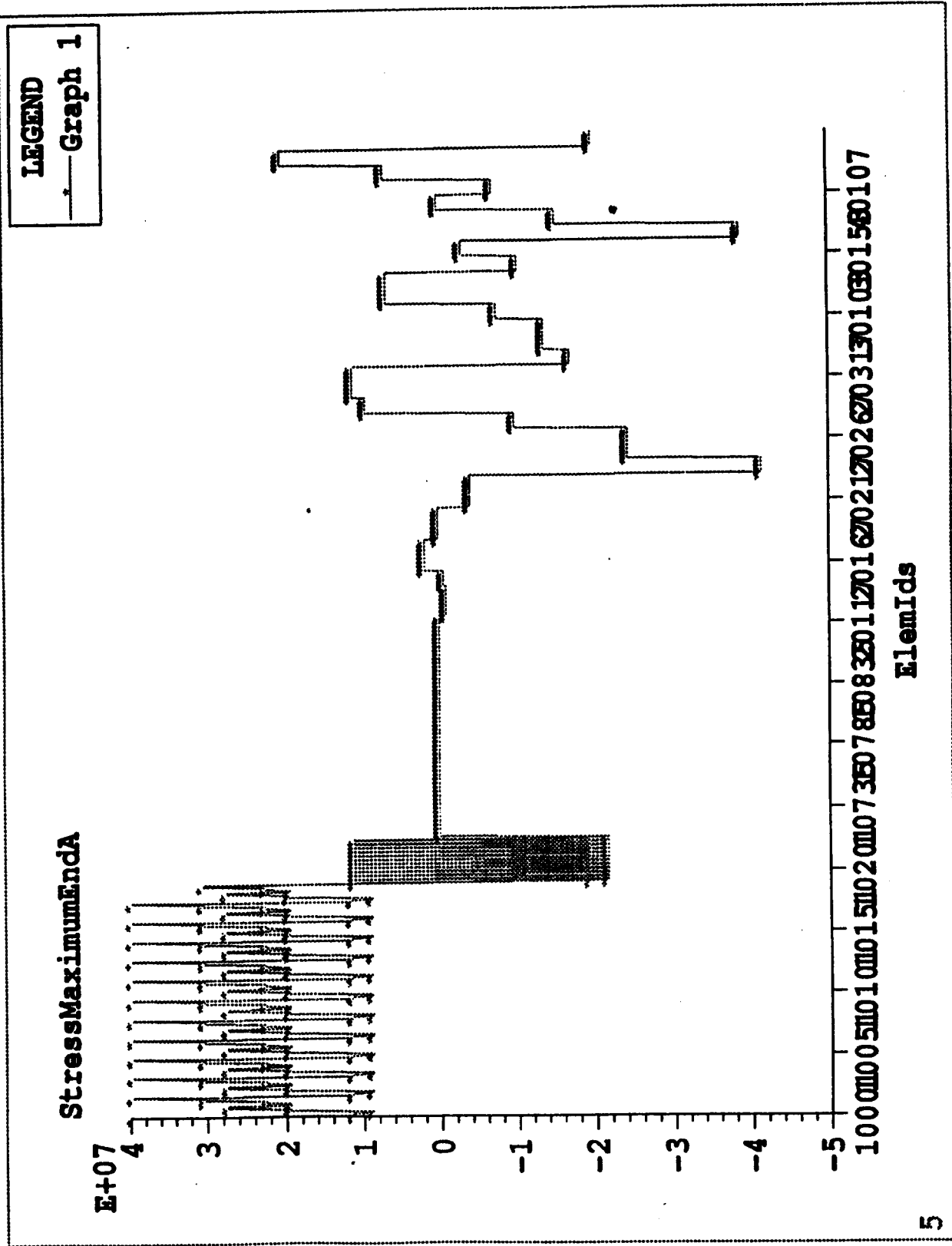


Figure 19 The stress of each member when the antenna under extreme loading is facing the dish

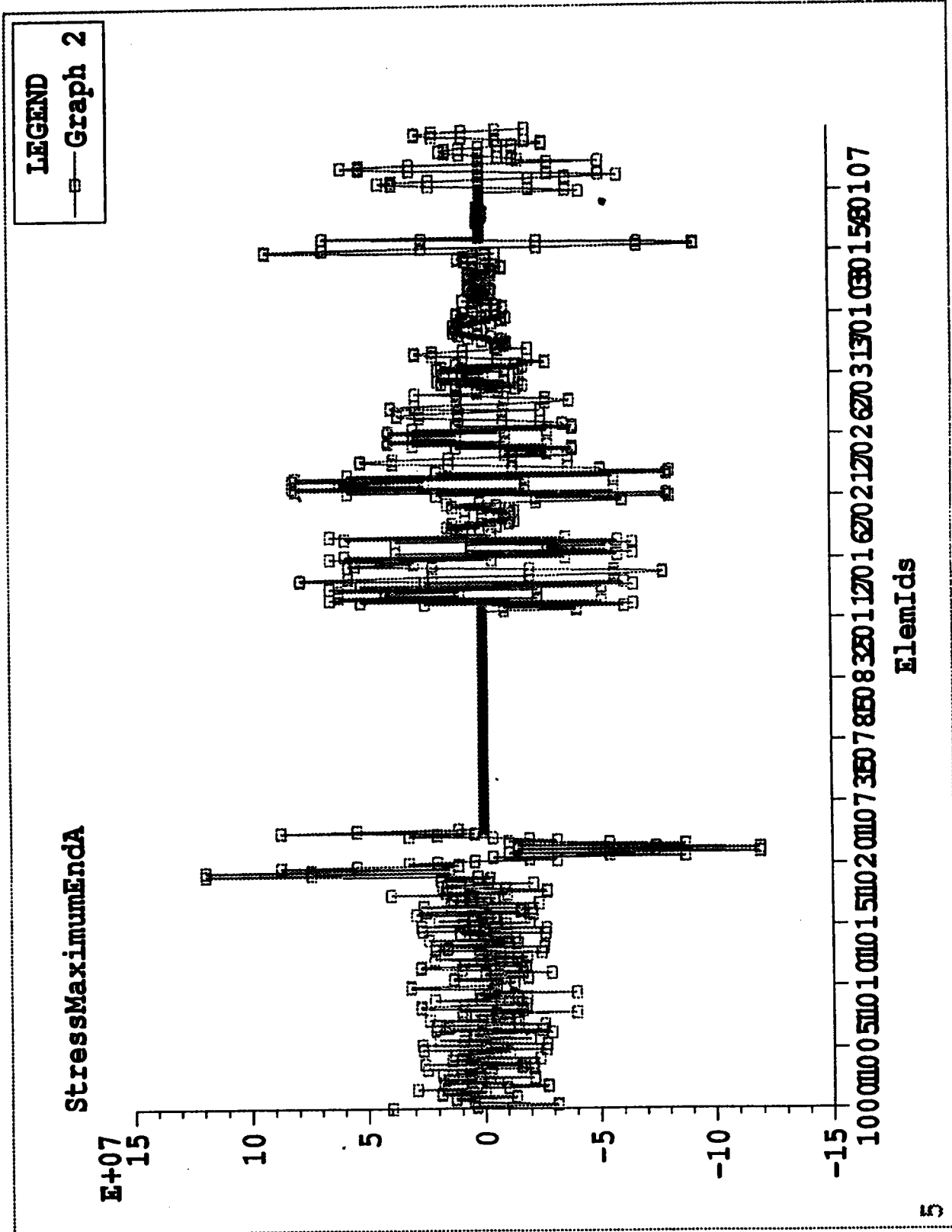


Figure 20 The stress of each member when the antenna under extreme loading is from side of the dish

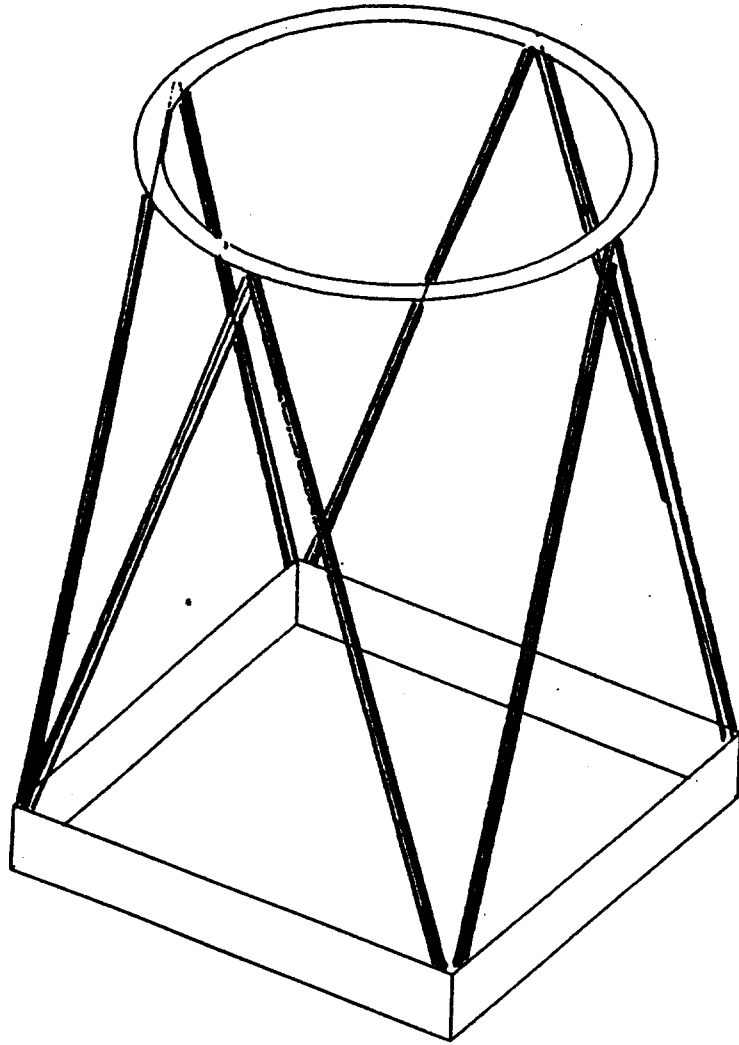


Figure A1 Serrurier truss structure used in optical telescope tube

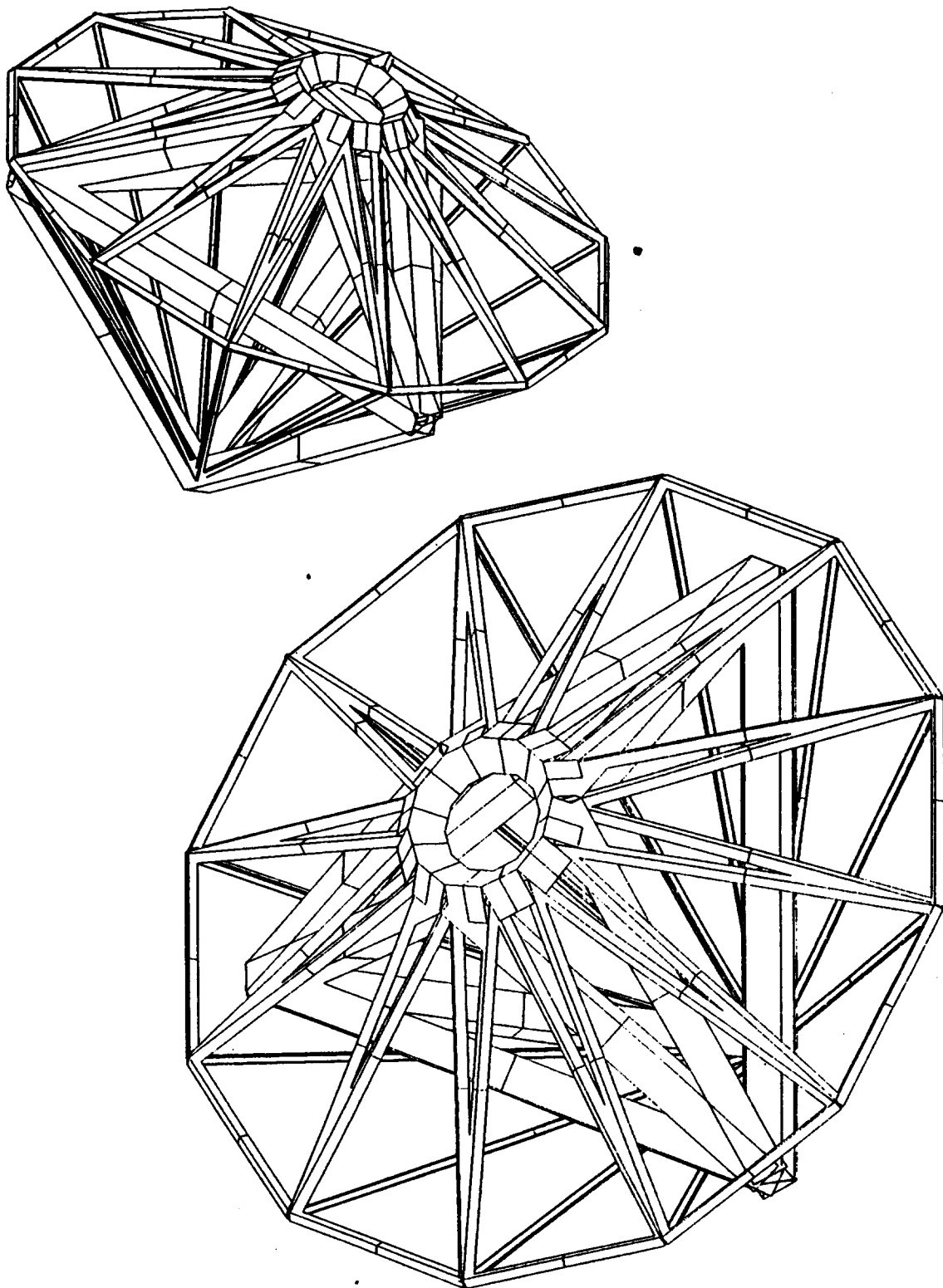


Figure A2 Serrurier-type trusses used at MMA antenna backup structure

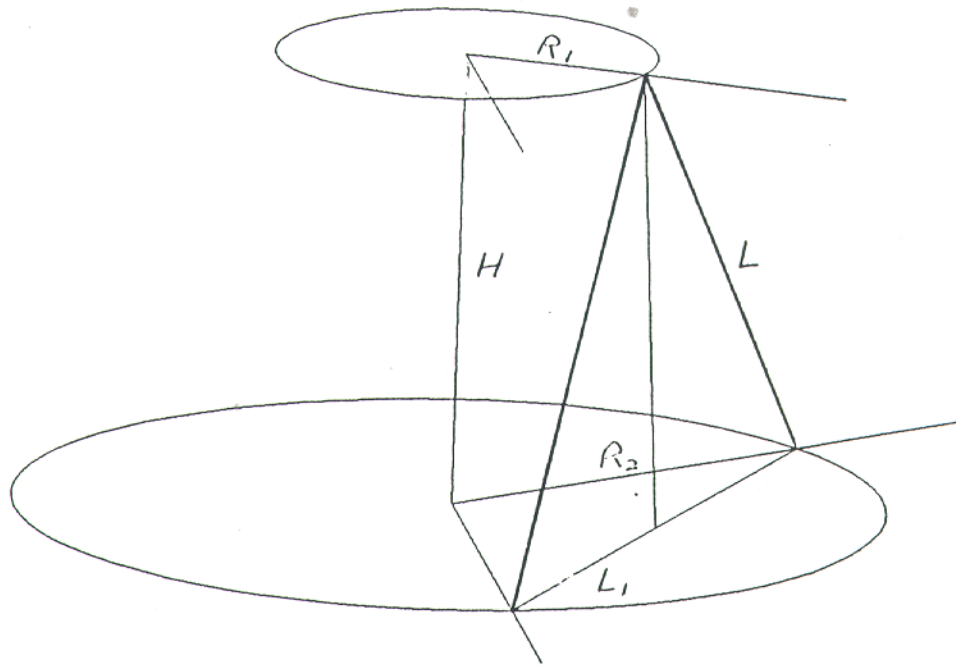


Figure A3 Truss parameters definition

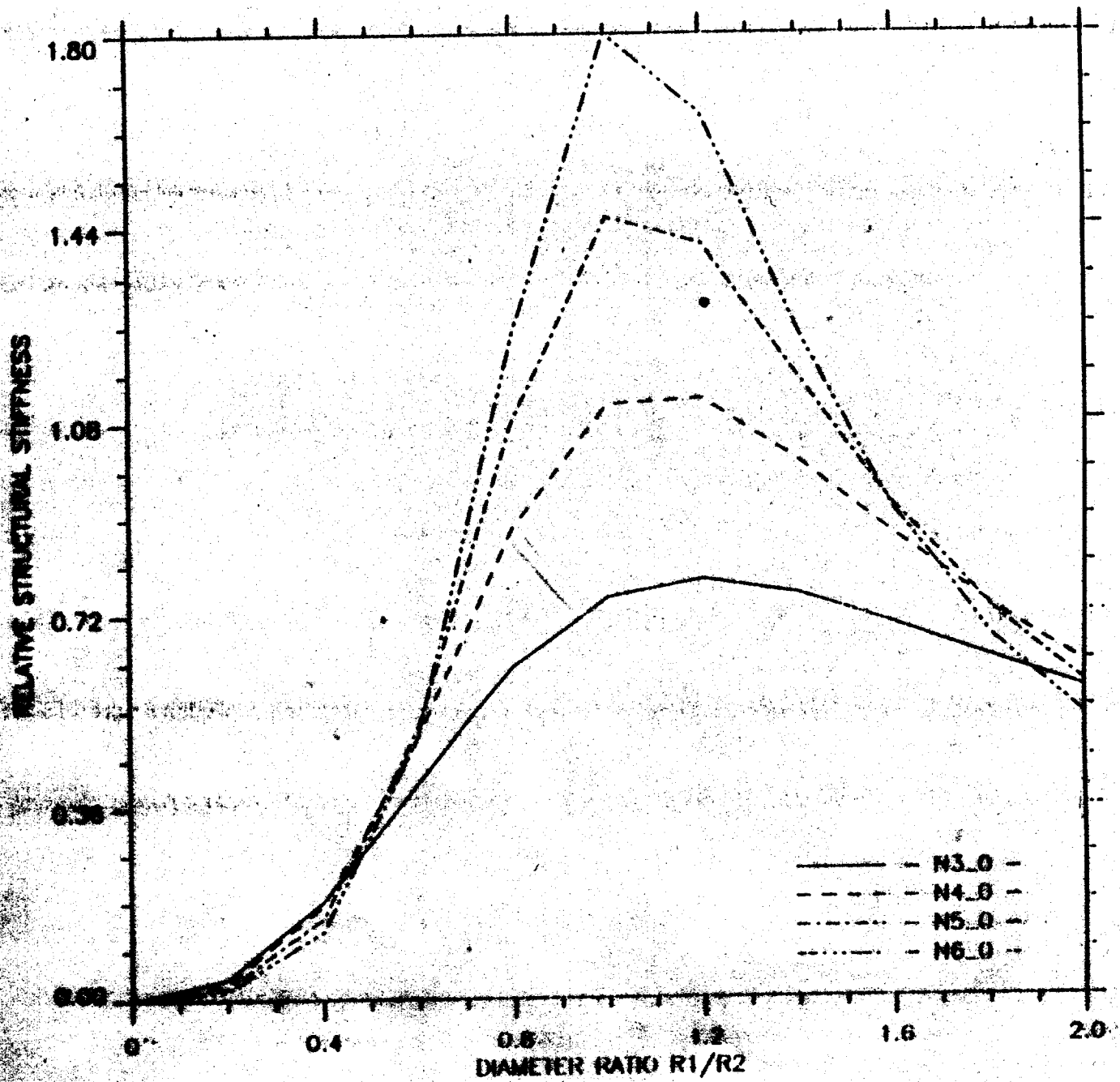


Figure A4 Stiffness of truss structures with different side number when ζ is zero

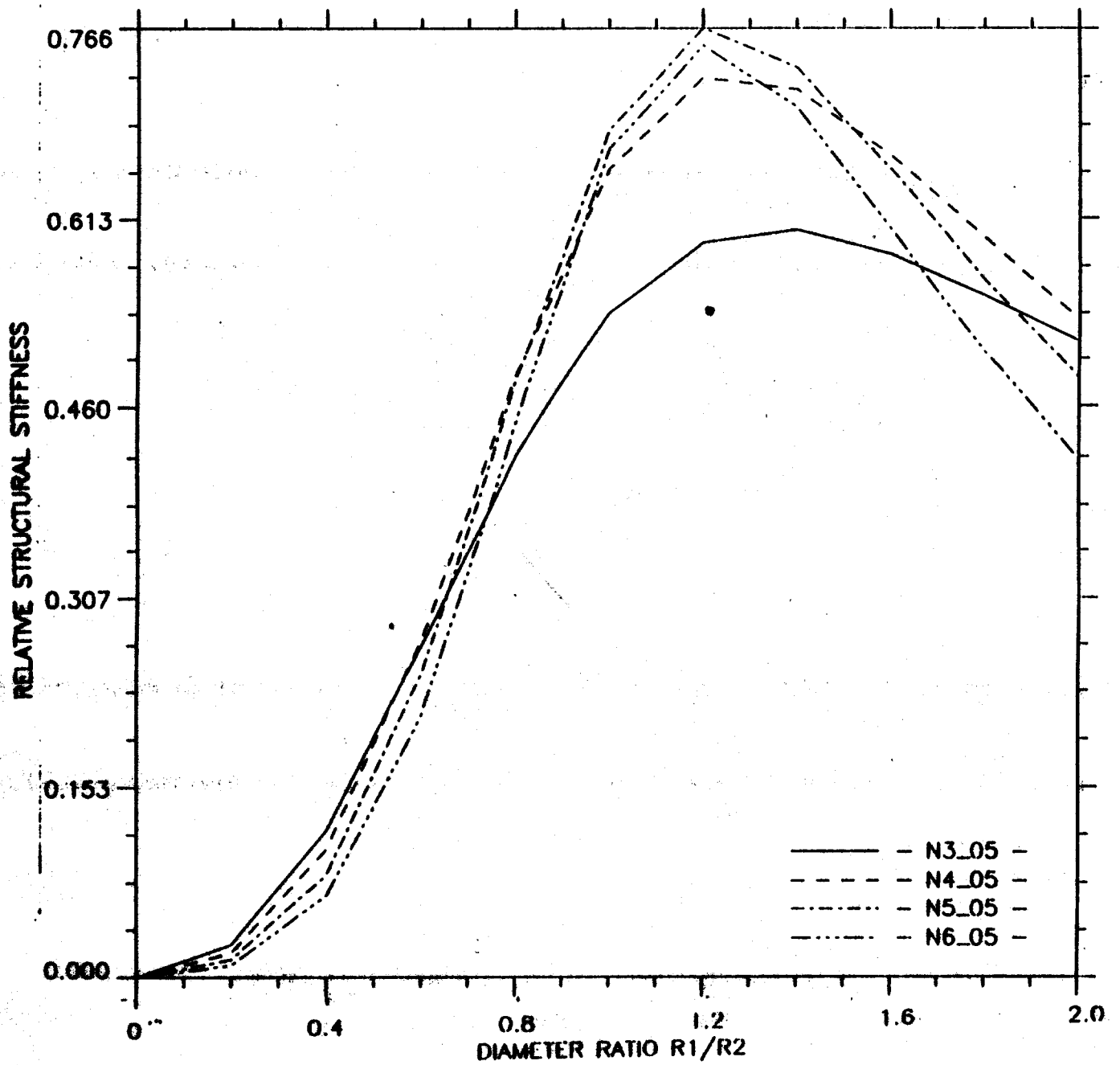


Figure A5 Stiffness of truss structures with different side number when ξ is 0.5

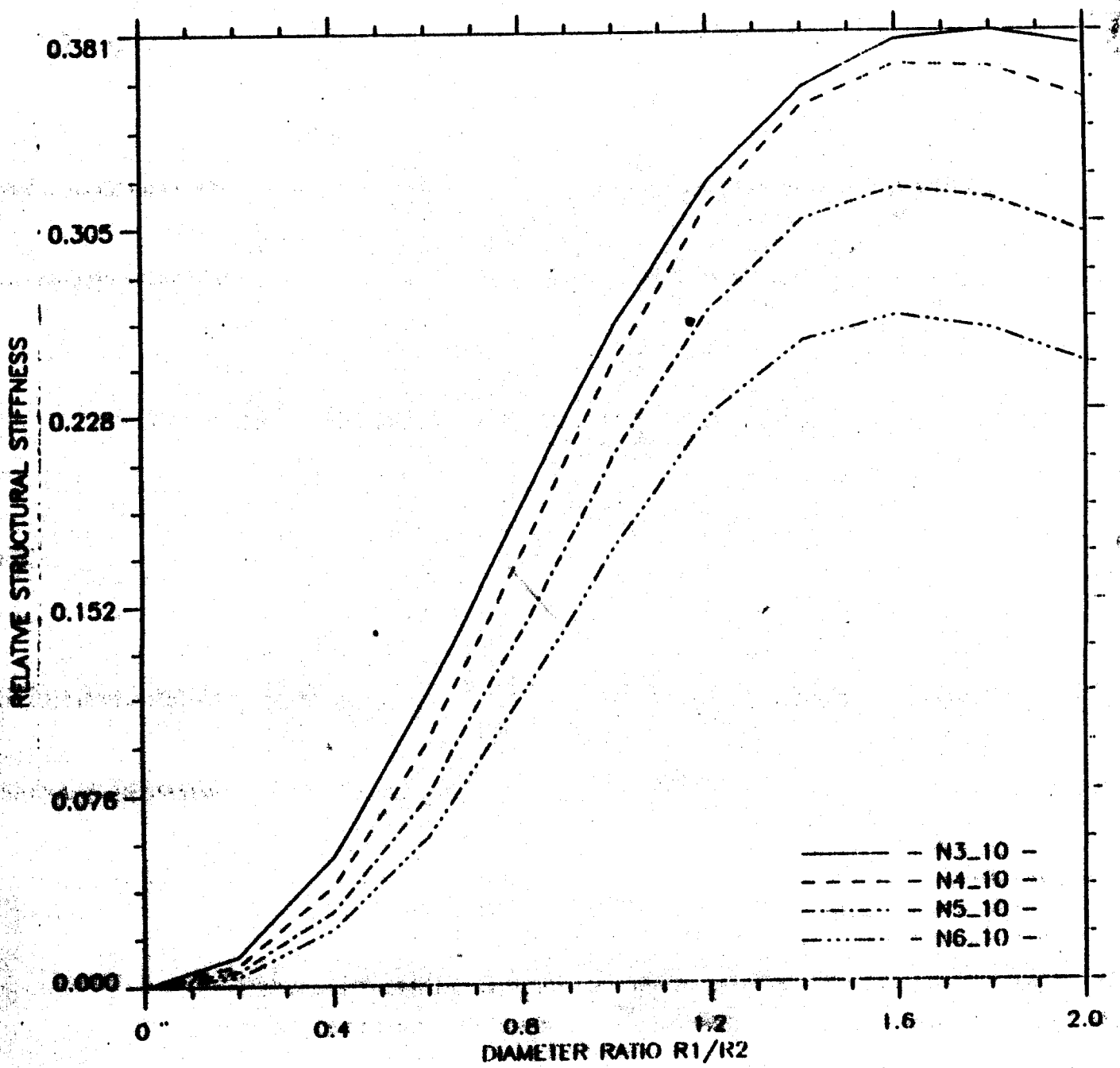


Figure A6 Stiffness of truss structures with different side number when ξ is 1.0

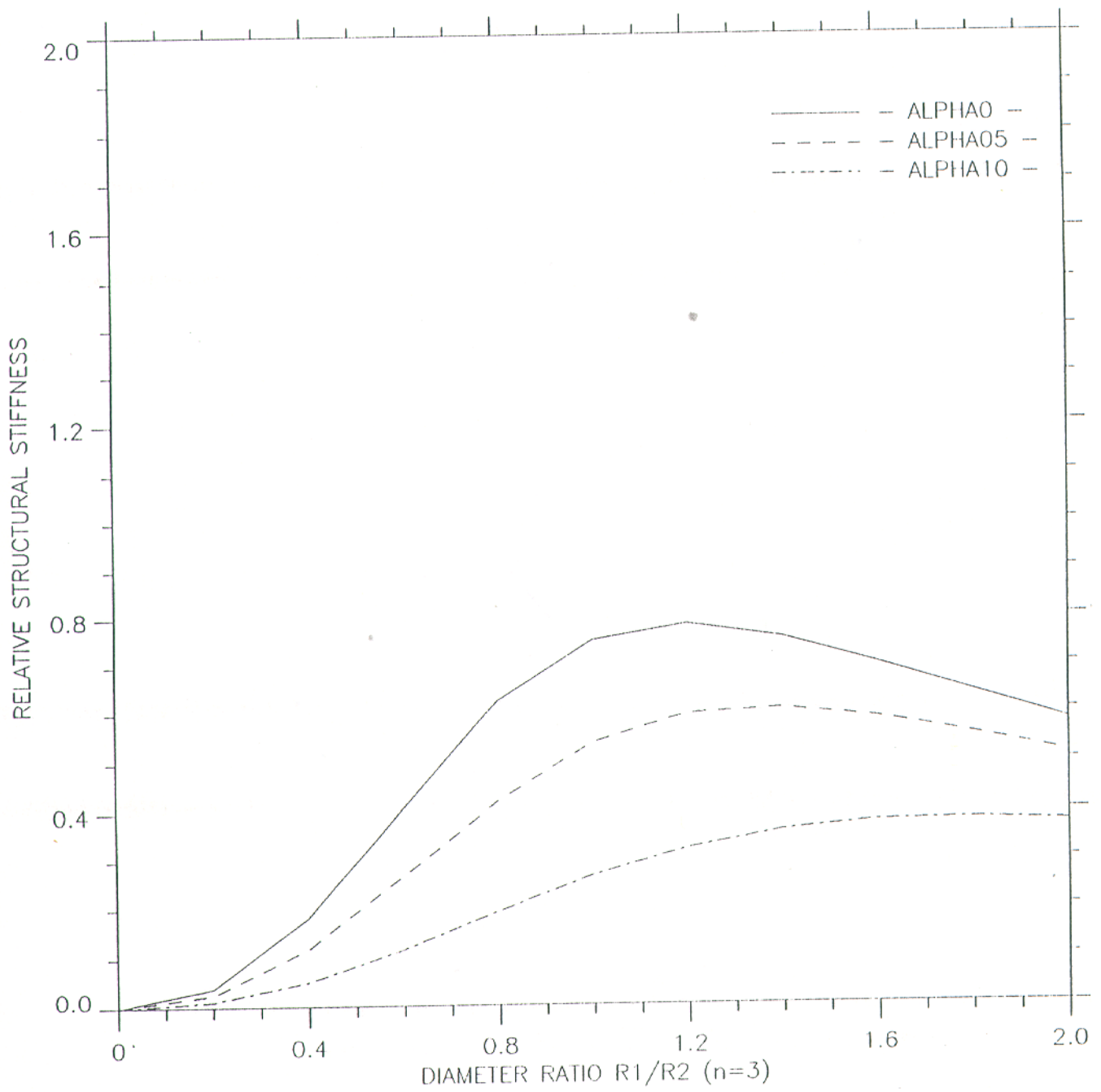


Figure A7 Stiffness of three side six beam truss structures with different ξ number

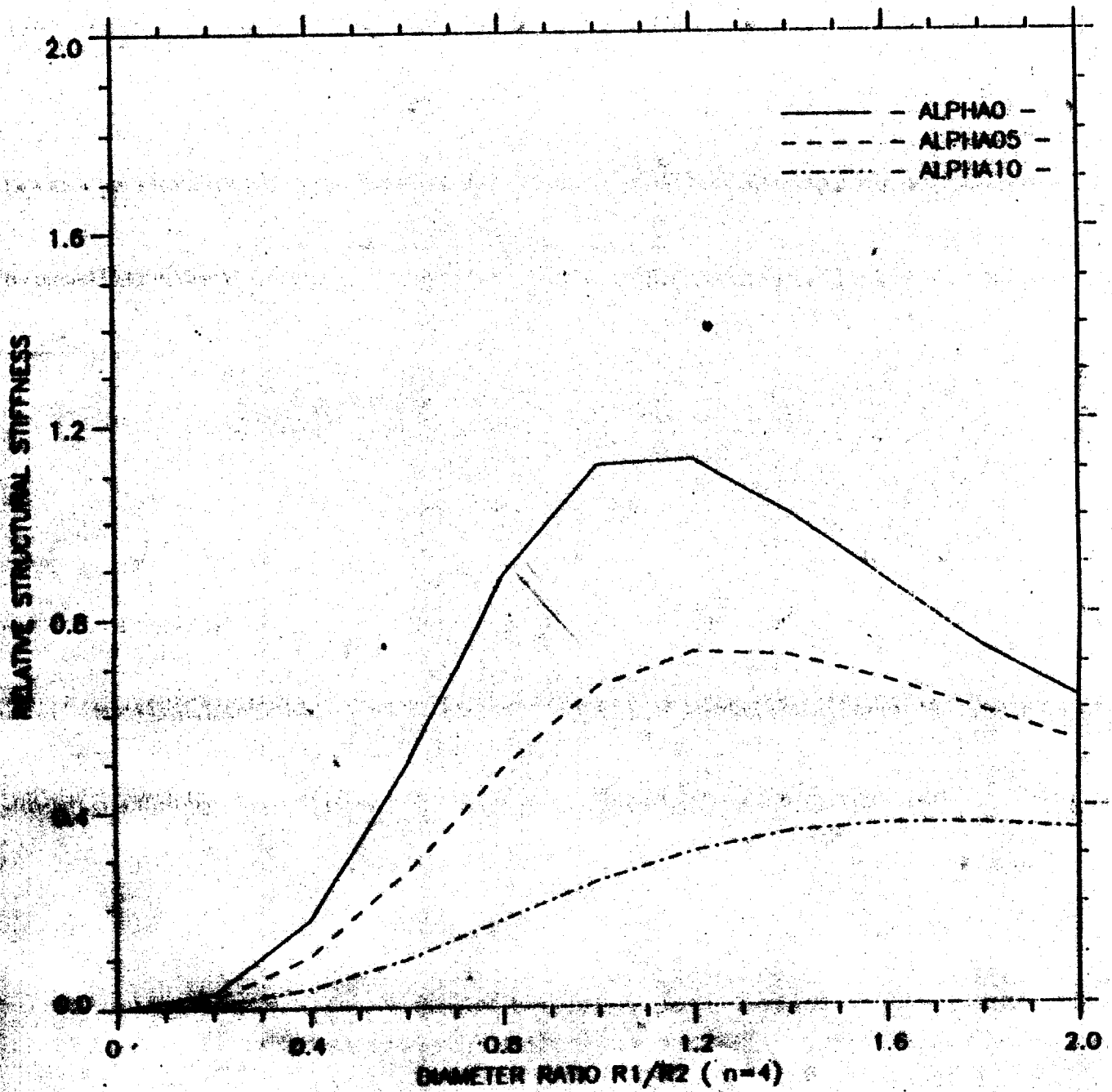


Figure A8 Stiffness of four side eight beam truss structures with different ξ number

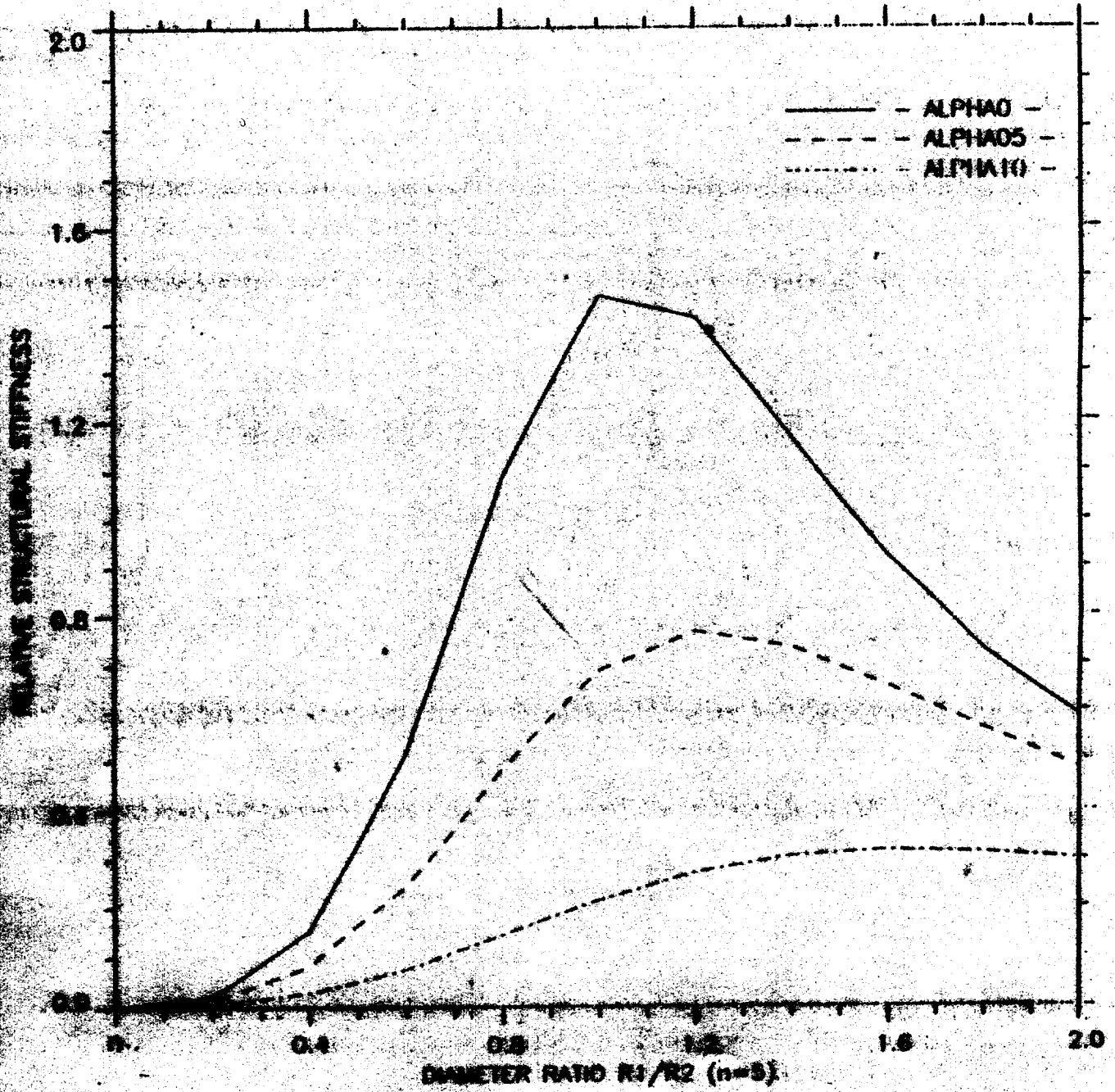


Figure A9 Stiffness of five side ten beam truss structures with different α number

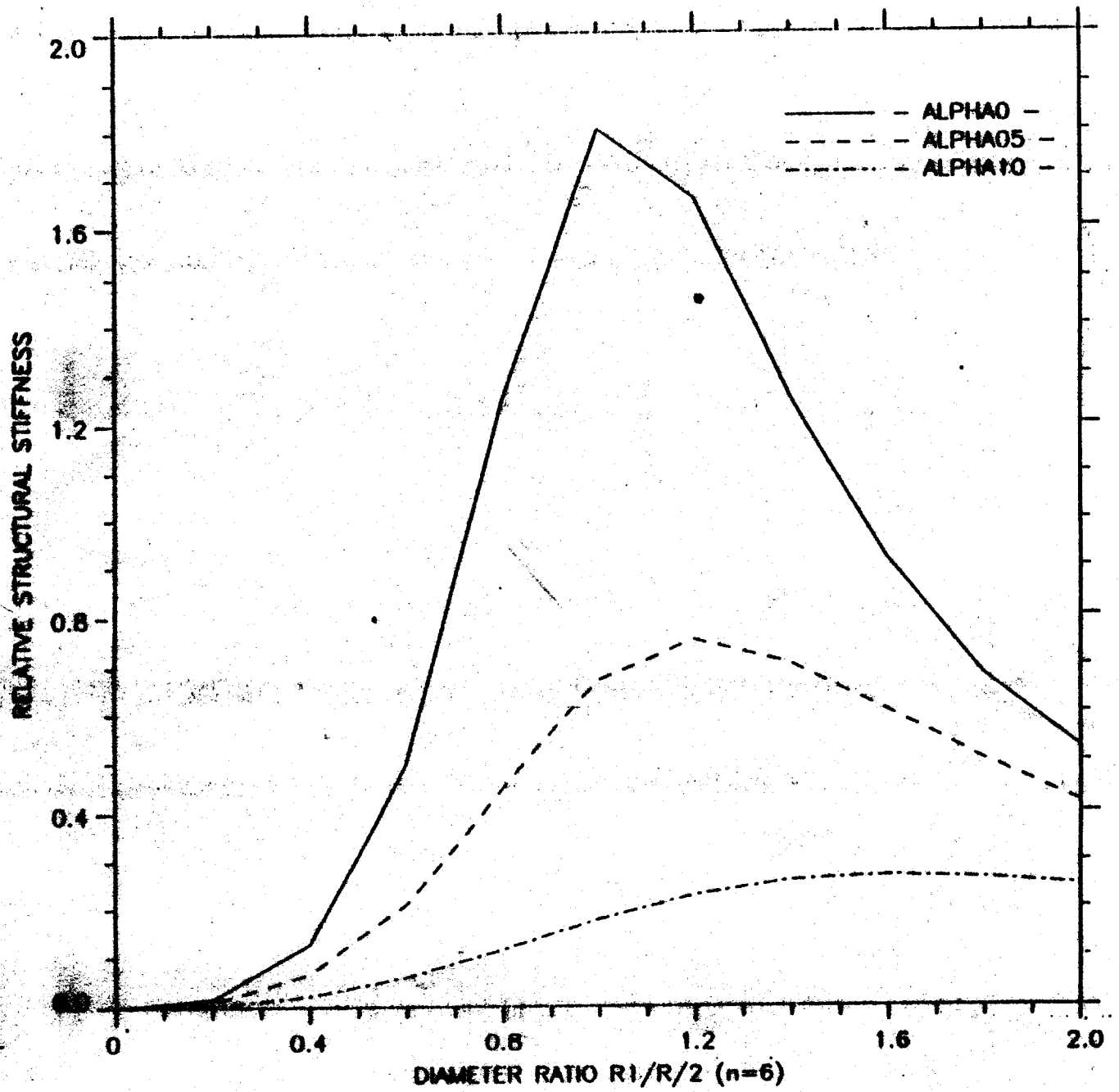


Figure A10 Stiffness of six side twelve beam truss structures with different ξ number